

Stability of discretized nonlinear elastic systems

Arnaud Lazarus^{*†}, Corrado Maurini^{*†}, and Sébastien Neukirch^{*†}

^{*} Sorbonne Universités, UPMC Univ Paris 06, UMR 7190,

Institut Jean Le Rond d'Alembert, F-75005, Paris, France

[†] Centre National de la Recherche Scientifique, UMR 7190,

Institut Jean Le Rond d'Alembert, F-75005 Paris, France

Abstract. The goal of these notes is to give a short introduction to the methods for the study of stability of elastic structures. We consider only the finite-dimensional case, where the state of the system is represented by a discrete set of parameters. The core of the exposition focuses on the illustration of energetic methods where the equilibrium and stability are found by studying the point of stationarity and minima of a scalar function of the state parameters. After three introductory sections presenting the links between stability and energy minimisations (Section 2), potential energy (Section 3) and discretisation methods (Section 4), we detail the mathematical methods required to minimise a function of n variables (Section 5-8). We include the theory and recipes to deal with equality and inequality constraints, providing several examples of applications to simple structures. Hence, we show how to classify regular and singular points (bifurcations) in force-displacement diagrams (Section 9) and give a fully worked example with several degrees of freedom (Section 10). Section 11 presents through an example the dynamical theory of stability including Floquet theory for systems with periodic coefficients. Finally, Section 12 shows how energetic methods can be applied to the study of material instabilities, by considering the case of springs with irreversible damage.

Contents

1	Introduction	3
2	Energy minimization and dynamical systems	3
3	Potential energy for an elastic beam	4
4	Three ways to discretize a continuous system	5
5	Minimum, maximum, extremum	8
6	Minimization without constraints	10
7	Minimization with equality constraints	13
8	Minimization with inequality constraints	18
9	Bifurcation diagrams	23
10	Buckling and post-buckling of a discrete beam on an elastic foundation	26
11	Dynamical stability	29
12	Material instabilities	45
	Bibliography	53

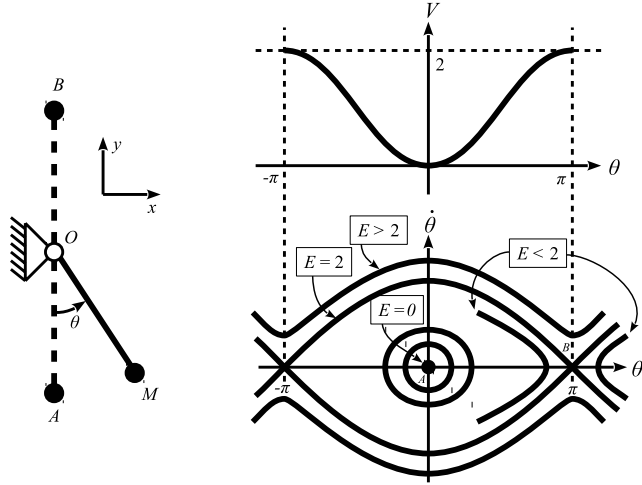


Figure 1. Dynamics of a simple pendulum. Associated potential energy $V(\theta)$ and phase plane $(\theta, \dot{\theta})$.

1 Introduction

We study the equilibrium and stability of nonlinear systems. Nonlinearity has two main consequences: (i) closed-form solutions are the exception and numerical methods have to be used; and (ii) unicity is lost, that is several solutions may exist for the same loading. While the ubiquity of computers reduces the importance of the first consequence, the second raises questions such as: which solution is to be considered? Which ones are stable? etc.

We restrict to the conservative case, where for example there is no friction, no viscous force (apart from Section 11 when dynamical stability will be introduced). Hence internal and external forces derive from potential energies, for example $1/2 \int_0^L \kappa^2 ds$ (curvature strain energy in a beam), mgz (gravitational energy), $-\mathbf{F} \cdot \mathbf{OA}$ (work of external load). Hence we do not consider follower or gyroscopic loads (see for example Ziegler (1977) or Bigoni (2012)).

2 Energy minimization and dynamical systems

We follow the principle stating that in conservative systems a stable equilibrium corresponds to a local minimum of the potential energy. In this

section we relate this energy-based stability criterion to the study of stability through the dynamics of the system.

We consider a simple pendulum, a punctual mass M fixed at the end of a massless rigid bar of length L , see Figure 1. The dynamics of the system obeys

$$\frac{d^2\theta}{dt^2} = -\sqrt{\frac{g}{L}} \sin \theta \quad (1)$$

where g is the acceleration of gravity. Using the dimensionless time $\tau := t \sqrt{L/g}$, Eq. (1) writes $\ddot{\theta} + \sin \theta = 0$, where $() := d/d\tau$. This equation is integrated once to yield

$$\frac{1}{2} \dot{\theta}^2 + 1 - \cos \theta = E \quad (2)$$

where the integration constant E is the total mechanical energy of the system, the sum of the kinetic energy $T = \frac{1}{2}\dot{\theta}^2$ and the potential energy $V = 1 - \cos \theta$, that is $E = T + V$. In figure 1 the stable (respectively unstable) equilibrium position A (resp. B) clearly appears as the local minimum (resp. maximum) of the potential energy V . Trajectories corresponding to the dynamics of the system for all possible initial conditions are drawn in the phase space $(\theta, \dot{\theta})$. There, equilibrium are points and the stable equilibrium A has closed trajectories in its neighborhood: perturbation of the equilibrium A leads to small vibrations around the position $\theta_A = 0$. The unstable equilibrium B has escaping trajectories in its neighborhood: some perturbations lead to evolution of the system far from B .

3 Potential energy for an elastic beam

In order to illustrate the theory, we focus on a simple elastic system : an elastic beam bent in the (x, y) plane, see Figure 2. The potential energy is then given by the functional (Audoly and Pomeau, 2010)

$$V[\theta] = \frac{1}{2} EI \int_0^L \theta'(s)^2 ds + P \int_0^L \cos \theta(s) ds \quad (3)$$

the first term being the internal strain energy and the second term the work done by the external applied load P . For the two cases in Figure 2, in the minimization process we have to take boundary (4) and/or integral conditions (5) into account:

$$\theta(0) = 0 \quad (4)$$

$$y(L) = 0 \text{ that is } \int_0^L \sin \theta(s) ds = 0 \quad (5)$$

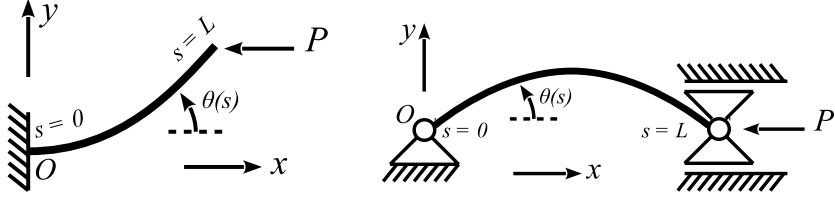


Figure 2. Elastic beams buckling in the plane. (Left) Clamped-free boundary conditions. (Right) Pinned-pinned boundary conditions.

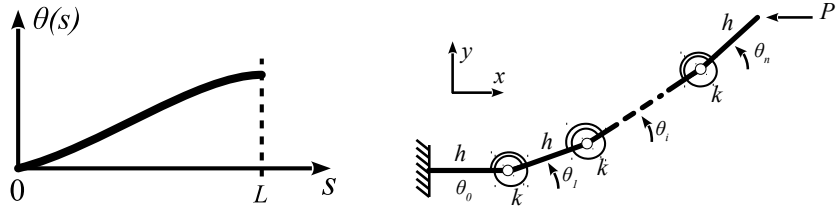


Figure 3. (Left) Solution $\theta(s)$ for the configuration in Figure 2-Left. (Right) A system of rigid bars linked by spiral springs.

4 Three ways to discretize a continuous system

4.1 Finite differences

Using $s_i = ih$, with $i \in (0, n + 1)$, and $s_{n+1} = L$, we apply a finite differences scheme for the derivative of $\theta(s)$, $\theta'(s) \simeq (\theta_{i+1} - \theta_i)/h$. We then apply the rectangle rule for integration and the energy functional (3) becomes:

$$V \simeq V_{\text{fd}} = \frac{1}{2} EI \sum_{i=0}^{n-1} \left(\frac{\theta_{i+1} - \theta_i}{h} \right)^2 h + P \sum_{i=0}^n \cos \theta_i h \quad (6)$$

We introduce dimensionless variables:

$$v = \frac{1}{n+1} \frac{V_{\text{fd}} L}{EI} = \frac{1}{2} \sum_{i=0}^{n-1} (\theta_{i+1} - \theta_i)^2 + \frac{p}{(n+1)^2} \sum_{i=0}^n \cos \theta_i \quad (7)$$

where $p = \frac{PL^2}{EI}$.

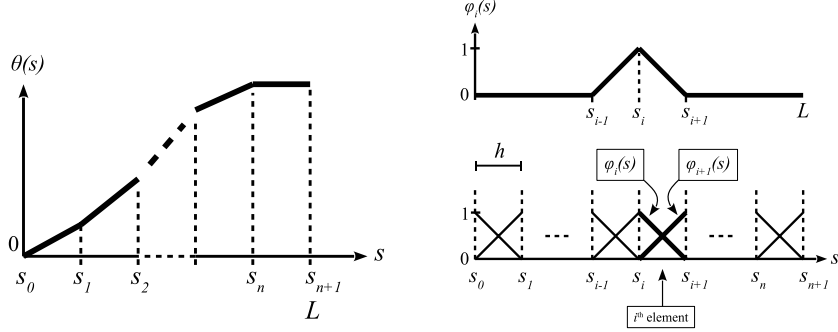


Figure 4. (Right) Piecewise linear approximation of the solution $\theta(s)$ shown in Figure 3-Left. (Left) A triangle base function, and the partitioning of the interval $(0, L)$ into $n + 1$ subintervals (or elements).

This is equivalent to the energy of a system of $n + 1$ rigid bars linked by spiral springs (see Figure 3):

$$V_{\text{bars}} = \frac{1}{2}k \sum_{i=0}^{n-1} (\theta_{i+1} - \theta_i)^2 + Ph \sum_{i=0}^n \cos \theta_i \quad (8)$$

where the spiral spring stiffness is k and the rigid bars have length h . The equivalence $V_{\text{bars}} = V_{\text{fd}}$ is obtained using $EI = k h$ and $L = (n + 1)h$.

4.2 Finite elements

In the former section, the solution $\theta(s)$ was approximated by a discontinuous piecewise constant function. Here we look for a continuous piecewise linear approximation. We therefore introduce triangle functions that take the value 1 at their center and have a compact support, see Figure 4. The interval $(0, L)$ is split into $n + 1$ elements of size h . The i^{th} element corresponds to $s \in (s_i, s_{i+1})$, with $s_i = i h$. The triangle functions $\varphi_i(s)$ span over elements $i - 1$ and i , with $\varphi_i(s_i) = 1$. Consequently, in the i^{th} element the two basis functions that are non zero are:

$$\varphi_i(s) = \frac{s_{i+1} - s}{h} \quad (9a)$$

$$\varphi_{i+1}(s) = \frac{s - s_i}{h} \quad (9b)$$

And in this element the approximation to the function $\theta(s)$ is given by

$$\theta_{\text{fe}}(s) = c_i \varphi_i(s) + c_{i+1} \varphi_{i+1}(s) \quad (10)$$

where the boundary condition $\theta'(L) = 0$ imposes $c_{n+1} = c_n$. Putting this ansatz in the functional (3) we obtain

$$\begin{aligned} v &= \frac{1}{n+1} \frac{VL}{EI} \\ &= \frac{1}{2} \sum_{i=0}^{n-1} (c_{i+1} - c_i)^2 + \frac{p}{(n+1)^2} \sum_{i=0}^{n-1} \frac{\sin c_{i+1} - \sin c_i}{c_{i+1} - c_i} + \frac{p}{(n+1)^2} \cos c_n \end{aligned} \quad (11)$$

At the discretization gets finer, the second term tends toward $\cos c_i$ and

$$v \xrightarrow{h \rightarrow 0} \frac{1}{2} \sum_{i=0}^{n-1} (c_{i+1} - c_i)^2 + \frac{p}{(n+1)^2} \sum_{i=0}^n \cos c_i \quad (12)$$

which is the same result as (7) with $\theta_i = c_i$.

4.3 Spectral decomposition

A third way to discretize the system in Figure 2-Left is to use the first n buckling modes as a functional basis and decompose the solution in this basis, see Figure 5. Here we use $n = 2$, the buckling modes are

$$\theta_1(s) = \sin \frac{\pi}{2} s \quad (13a)$$

$$\theta_2(s) = \sin \frac{3\pi}{2} s \quad (13b)$$

The approximate solution is then written as

$$\theta(s) = \alpha \sin \frac{\pi}{2} s + \beta \sin \frac{3\pi}{2} s \quad (14)$$

We inject this ansatz into the functional (3) and obtain:

$$\begin{aligned} v(\alpha, \beta) &= \frac{1}{2} \int_0^1 \left(\alpha \frac{\pi}{2} \cos \frac{\pi}{2} s + \beta \frac{3\pi}{2} \cos \frac{3\pi}{2} s \right)^2 ds \\ &\quad + P \int_0^1 \cos \left[\alpha \sin \frac{\pi}{2} s + \beta \sin \frac{3\pi}{2} s \right] ds \end{aligned} \quad (15)$$

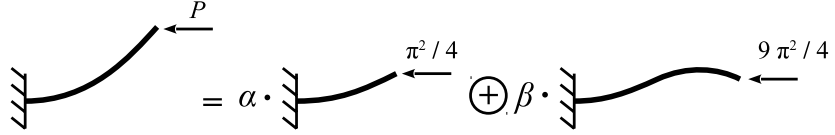


Figure 5. Spectral discretization based on the first two buckling modes.

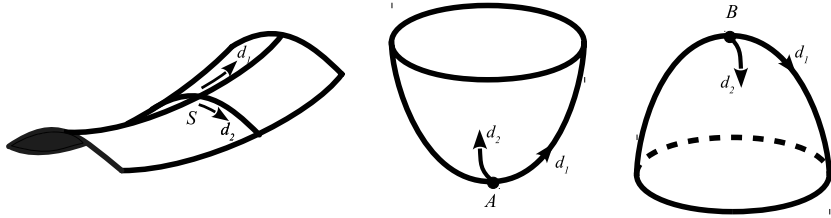


Figure 6. A saddle point (S), a minimum (A), and a maximum (B)

The first integral is easily evaluated but not the second one. Gauss-Legendre integration is then used, with 2 points. We obtain

$$v(\alpha, \beta) = \frac{\pi^2}{16}(\alpha^2 + 9\beta^2) + \frac{P}{2} [\cos(0.95\alpha - 0.54\beta) + \cos(0.33\alpha - 0.84\beta)] \quad (16)$$

5 Minimum, maximum, extremum

Once the discretization is achieved, we are left with a function $V(\mathbf{x})$, where $V \in \mathbb{R}$ and $\mathbf{x} \in \mathbb{R}^n$, and we look for the point(s) for which V is locally minimum. Examples are:

- $V(x_1, x_2) = x_1^2 + x_2^2$ has a *global* minimum at $(x_1, x_2) = (0, 0)$.
- $V(x_1, x_2) = x_1^2 - x_2^2$ has no *global* or *local* minimum. The point $(x_1, x_2) = (0, 0)$ is a saddle point.
- $V(x) = x^2 - x^4$ has a *local* minimum at $x = 0$.

Stated in this way the problem of the equilibrium and stability of an elastic structure becomes a problem of nonlinear optimization. We therefore use methods of nonlinear programming, see for example Luenberger and Ye (2008).

5.1 Values of a function in one direction

We are given a function $V(\mathbf{x})$, where $V \in \mathbb{R}$ and $\mathbf{x} \in \mathbb{R}^n$. We are interested to know if the point \mathbf{x}_0 is a local minimum. Instead of looking at the values of V all around \mathbf{x}_0 , we *restrict* to the values taken by V in the direction \mathbf{d} . That is we study the one-variable function

$$V(\mathbf{x}_0)(\mathbf{d}) := V(\mathbf{x}_0 + \epsilon \mathbf{d}) = V(\epsilon) \text{ for } \epsilon \in \mathbb{R} \quad (17)$$

Example: For the function $V(x_1, x_2) = x_1^2 - x_2^2$, the point $(x_1, x_2) = (0, 0)$ is a saddle point:

- If we study $V(\mathbf{x}_0)(\mathbf{d})$ with $x_0 = (0, 0)$ and $\mathbf{d} = (1, 0)$. We have $V(\mathbf{x}_0)(\mathbf{d}) = V(\epsilon) = \epsilon^2$. In this direction we have a local minimum.
- If we study $V(\mathbf{x}_0)(\mathbf{d})$ with $x_0 = (0, 0)$ and $\mathbf{d} = (0, 1)$. We have $V(\mathbf{x}_0)(\mathbf{d}) = V(\epsilon) = -\epsilon^2$. In this direction we have a local maximum.

5.2 Derivative of a function in one direction

We now want to study the derivative with regard to ϵ of $V(\epsilon)$, that is $V'(\epsilon)$. This is the directional derivative of $V(\mathbf{x})$ in the direction \mathbf{d} , at the point \mathbf{x}_0 :

$$V'(\mathbf{x}_0)(\mathbf{d}) := \frac{d}{d\epsilon} V(\mathbf{x}_0 + \epsilon \mathbf{d}) \Big|_{\epsilon=0} \quad (18)$$

Example : for the function $V(x_1, x_2) = x_1^2 - x_2^2$,

- we compute the directional derivative at the point $(x_1, x_2) = (0, 0)$ in the direction $d = (1, 0)$. We have $V(\epsilon) = V(\mathbf{x}_0 + \epsilon \mathbf{d}) = \epsilon^2$, $V'(\epsilon) = 2\epsilon$, and finally $V'(\mathbf{x}_0)(\mathbf{d}) = V'(\epsilon)|_{\epsilon=0} = 0$.
- we compute the directional derivative at the point $(x_1, x_2) = (1, 0)$ in the direction $d = (1, 2)$. We have $V(\epsilon) = V(\mathbf{x}_0 + \epsilon \mathbf{d}) = -3\epsilon^2 + 2\epsilon + 1$, and $V'(\mathbf{x}_0)(\mathbf{d}) = V'(\epsilon)|_{\epsilon=0} = 2$.

5.3 Directional derivative and gradient

We consider $V(\mathbf{x}_0 + \epsilon \mathbf{d})$ with $\mathbf{x}_0 = (x_1^0, x_2^0)$ and $\mathbf{d} = (d_1, d_2)$. The Taylor expansion around \mathbf{x}_0 for small ϵ writes:

$$\begin{aligned} V(x_1^0 + \epsilon d_1, x_2^0 + \epsilon d_2) &= V(x_1^0, x_2^0) + \epsilon \frac{\partial V}{\partial x_1} \Big|_{\mathbf{x}=\mathbf{x}_0} d_1 + \epsilon \frac{\partial V}{\partial x_2} \Big|_{\mathbf{x}=\mathbf{x}_0} d_2 + O(\epsilon^2) \\ &= V(x_1^0, x_2^0) + \epsilon \nabla V|_{\mathbf{x}_0} \cdot \mathbf{d} + O(\epsilon^2) \end{aligned} \quad (19)$$

where $\nabla := \frac{\partial}{\partial \mathbf{x}}$.

5.4 Taylor expansion up to order two

The Taylor expansion up to second order is:

$$\begin{aligned} V(x_1^0 + \epsilon d_1, x_2^0 + \epsilon d_2) &= V(x_1^0, x_2^0) + \epsilon \nabla V|_{\mathbf{x}_0} \cdot \mathbf{d} + \frac{1}{2} \epsilon^2 d_1^2 \frac{\partial^2 V}{\partial x_1^2} \Big|_{\mathbf{x}=\mathbf{x}_0} \\ &\quad + \epsilon^2 d_1 d_2 \frac{\partial^2 V}{\partial x_1 \partial x_2} \Big|_{\mathbf{x}=\mathbf{x}_0} + \frac{1}{2} \epsilon^2 d_2^2 \frac{\partial^2 V}{\partial x_2^2} \Big|_{\mathbf{x}=\mathbf{x}_0} \end{aligned} \quad (20)$$

The second order term can be written as:

$$\frac{1}{2} \epsilon^2 \mathbf{d} \cdot \mathbf{H}_0 \cdot \mathbf{d} \quad (21)$$

where $\mathbf{H} = \mathbf{H}(\mathbf{x})$ is the Hessian matrix, $H_{ij} = \frac{\partial^2 V}{\partial x_i \partial x_j}$, and \mathbf{H}_0 means \mathbf{H} when evaluated on $\mathbf{x} = \mathbf{x}_0$.

6 Minimization without constraints

6.1 First derivative

We are given a function $V(\mathbf{x})$, where $V \in \mathbb{R}$ and $\mathbf{x} \in \mathbb{R}^n$ and we require the point \mathbf{x}_0 to be a local minimum. That is we want

$$V(\mathbf{x}) \geq V(\mathbf{x}_0) \quad \forall \mathbf{x} \text{ near } \mathbf{x}_0 \quad (22)$$

Hence we write $\mathbf{x} = \mathbf{x}_0 + \epsilon \mathbf{d}$ and consider small ϵ and all possible directions \mathbf{d} (but not $\mathbf{d} = \mathbf{0}$). Using (19), the condition (22) yields

$$\epsilon \frac{\partial V}{\partial \mathbf{x}} \Big|_{\mathbf{x}_0} \cdot \mathbf{d} \geq 0 \quad \forall \epsilon \text{ and } \forall \mathbf{d} \quad (23)$$

As positive and negative ϵ can be considered this implies $\frac{\partial V}{\partial \mathbf{x}} \Big|_{\mathbf{x}_0} \cdot \mathbf{d} = 0 \quad \forall \mathbf{d}$, and finally

$$\frac{\partial V}{\partial \mathbf{x}} \Big|_{\mathbf{x}_0} = \mathbf{0} \quad (24)$$

This is a necessary condition in order to have a minimum at \mathbf{x}_0 . If V is a potential energy of a system, then these n equations for the n unknowns (x_1, x_2, \dots, x_n) are the equilibrium equations.

6.2 Second derivative

Having solved the (nonlinear) equilibrium equations (24) and found one or more solutions $\mathbf{x}_A, \mathbf{x}_B, \dots$, we want to test whether these solutions are

stable, that is whether they correspond to local minimum of the energy. As for these solutions the first derivative vanishes, we need to look at the second derivative term in (20). The requirement (22) for a minimum now yields:

$$\mathbf{d} \cdot \mathbf{H}_0 \cdot \mathbf{d} \geq 0 \quad \forall \mathbf{d} \quad (25)$$

A sufficient condition is

$$\mathbf{d} \cdot \mathbf{H}_0 \cdot \mathbf{d} > 0 \quad \forall \mathbf{d} \quad (26)$$

In the case where there is a \mathbf{d} for which $\mathbf{d} \cdot \mathbf{H}_0 \cdot \mathbf{d} = 0$, we cannot conclude and would have to compute higher orders. In the case there is one (or more) \mathbf{d} for which $\mathbf{d} \cdot \mathbf{H}_0 \cdot \mathbf{d} < 0$, then the point \mathbf{x}_0 is not a minimum.

Example: Minimize the function $V(x_1, x_2) = x_1^2 - x_2^2 + x_2^4$ in \mathbb{R}^2 .

6.3 Recipe

As the matrix \mathbf{H}_0 is symmetric, we can write it in its eigenspace. It is then diagonal with real entries, its eigenvalues λ_i with $i \in (1, n)$. In this representation, the condition (26) writes:

$$d_1^2 \lambda_1 + d_2^2 \lambda_2 + \dots + d_n^2 \lambda_n > 0 \quad \forall d_i \quad (27)$$

which means that we must have $\lambda_i > 0 \ \forall i$, that is all eigenvalues must be strictly positive.

Here is the procedure to follow when we have the potential energy $V(x)$ of a system to minimize:

- compute the equilibria, that is the solution(s) of $\frac{\partial V}{\partial \mathbf{x}} = \mathbf{0}$
- then, for each equilibrium solution:

- compute the matrix $H_{ij} = \frac{\partial^2 V}{\partial x_i \partial x_j}$, and evaluate it on the equilibrium solution, then compute its eigenvalues λ_i
- if $\lambda_i > 0 \ \forall i$ then the equilibrium is stable
- if there is one (or more) i such that $\lambda_i < 0$, then the equilibrium is unstable
- if the λ_i are all positive, but there is one (or more) i such that $\lambda_i = 0$, we cannot at this stage conclude on the stability.

6.4 Discrete vs. Continuous

If on the one hand we consider the continuous energy (3) and write Euler-Lagrange equations for it, we obtain

$$EI \theta''(s) + P \sin \theta(s) = 0 \quad (28)$$

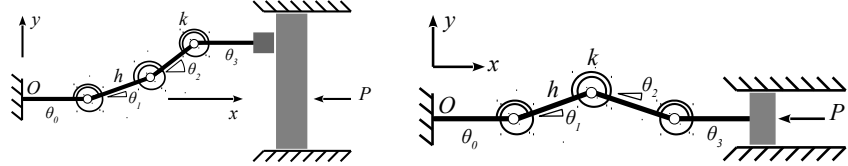


Figure 7. System of 4 bars linked by spiral springs. (Left) Ends are horizontal. (Right) Ends are horizontal and aligned

If now on the other hand we consider the discretized energy (6) and write the first derivative condition (24) we obtain

$$-EI \frac{\theta_{i+1} - 2\theta_i + \theta_{i-1}}{h} - Ph \sin \theta_i = 0 \quad (29)$$

and we see that (29) is the finite differences version of (28), showing that the discretization and minimization procedures are commutative operations:

$$\begin{array}{ccc} V[\theta(s)] & \xrightarrow{\text{Euler-Lagrange}} & EI\theta'' + P \sin \theta = 0 \\ \downarrow \text{finite diff.} & & \downarrow \text{finite diff.} \\ V(\theta_i) & \xrightarrow{\text{First derivative}} & EI \frac{\theta_{i+1} - 2\theta_i + \theta_{i-1}}{h^2} + P \sin \theta_i = 0 \end{array}$$

6.5 Example: The clamped beam

We here compute the buckling load of the two degrees of freedom system of Figure 7-Left. The energy of the system is

$$V = \frac{1}{2}k(\theta_1 - \theta_0)^2 + \frac{1}{2}k(\theta_2 - \theta_1)^2 + \frac{1}{2}k(\theta_3 - \theta_2)^2 + Ph(\cos \theta_0 + \cos \theta_1 + \cos \theta_2 + \cos \theta_3) \quad (30)$$

and the boundary conditions reads: $\theta_0 = 0 = \theta_3$. The variables are then (θ_1, θ_2) . We introduce dimensionless variables $v = V/k$ and $p = 16Ph/k$ in order to follow notations of equation (7). Equilibrium equations are

$$\frac{\partial v}{\partial \theta_1} = 2\theta_1 - \theta_2 - \frac{p}{16} \sin \theta_1 = 0 \quad (31a)$$

$$\frac{\partial v}{\partial \theta_2} = -\theta_1 + 2\theta_2 - \frac{p}{16} \sin \theta_2 = 0 \quad (31b)$$

One trivial solution is $\theta_1 = 0 = \theta_2$. We study its stability. The Hessian matrix is

$$\mathbf{H}_0 = \begin{pmatrix} 2 - p/16 & -1 \\ -1 & 2 - p/16 \end{pmatrix} \quad (32)$$

and has $\lambda_1 = 1 - p/16$ and $\lambda_2 = 3 - p/16$ as eigenvalues. We conclude the trivial solution is stable for $p < 16$ and unstable for $p > 16$. Buckling therefore happens at $p = 16$.

7 Minimization with equality constraints

Given a function $V(\mathbf{x})$, where $V \in \mathbb{R}$ and $\mathbf{x} \in \mathbb{R}^n$, we look for the point(s) for which V is locally minimum, but only for the point(s) that satisfy one (or more) constraints $g(\mathbf{x}) = 0$.

Example: Minimize $V(x_1, x_2) = x_1^2 + x_2^2$ in the subset where $g(x_1, x_2) = \frac{x_1 - 1}{1} = 0$.

7.1 First derivative

We are given a function $V(\mathbf{x})$ that is to be minimized in the subset where $g(\mathbf{x}) = 0$. We require the point \mathbf{x}_0 to be a local minimum by stating that for small ϵ

$$V(\mathbf{x} = \mathbf{x}_0 + \epsilon\mathbf{d}) \geq V(\mathbf{x}_0) \quad \forall \mathbf{x} \text{ such that } g(\mathbf{x}_0 + \epsilon\mathbf{d}) = 0 \quad (33)$$

This means that not all \mathbf{d} directions will be tested. Only the directions \mathbf{d} fulfilling

$$g(\mathbf{x}_0 + \epsilon\mathbf{d}) = g(\mathbf{x}_0) + \epsilon\nabla g|_{\mathbf{x}_0} \cdot \mathbf{d} + O(\epsilon^2) = 0 \quad (34)$$

will be tested. As in the unconstrained case, positive and negative ϵ can be considered. Therefore we need to have

$$\nabla V|_{\mathbf{x}_0} \cdot \mathbf{d} = 0 \quad \forall \mathbf{d} \text{ such that } \nabla g|_{\mathbf{x}_0} \cdot \mathbf{d} = 0 \quad (35)$$

This implies that ∇V and ∇g are colinear, that is there is a real number λ such that

$$\nabla V|_{\mathbf{x}_0} = \lambda \nabla g|_{\mathbf{x}_0} \quad (36)$$

The function g is given and ∇g defines a direction in space. The vectors \mathbf{d} perpendicular to the gradient of g are in the tangent (hyper-)plane of the surface $g = 0$ at point \mathbf{x}_0 , see Figure 8. The equilibrium equations are the n equations (36) plus $g(\mathbf{x}) = 0$, and the unknowns are the n components of \mathbf{x} plus the real number λ .

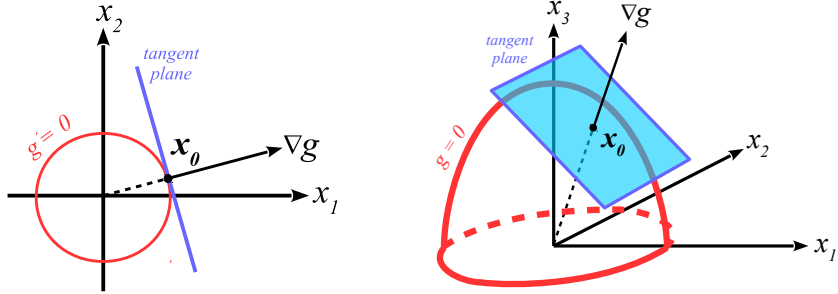


Figure 8. Tangent planes in 2D and 3D

A way to memorize Eq. (36) is through the introduction of the augmented energy $W = V - \lambda g$ and solve for $\nabla W = \mathbf{0}$. In such a view λ is called a Lagrange multiplier.

Example: We minimize $V(x_1, x_2) = x_1^2 + x_2^2$ under the constraint $g(x_1, x_2) = (x_1 - 1)^2 + (x_2 - 2)^2 - 1 = 0$. The first order condition $\nabla V = \lambda \nabla g$ has two solutions. The first one is point A such that $x_1^A = 1 - 1/\sqrt{5}$, $x_2^A = 2 - 2/\sqrt{5}$, $\lambda_A = 1 - \sqrt{5}$, and the second one is point B such that $x_1^B = 1 + 1/\sqrt{5}$, $x_2^B = 2 + 2/\sqrt{5}$, $\lambda_B = 1 + \sqrt{5}$.

7.2 Second derivative

For the second derivative, we need to consider a perturbation to the equilibrium solution \mathbf{x}_0 such that \mathbf{x} stays on the surface $g = 0$. Contrary to what was done in the unconstrained case we need to develop the perturbation to second order:

$$\mathbf{x} = \mathbf{x}_0 + \epsilon \mathbf{d} + \frac{1}{2} \epsilon^2 \mathbf{e} + O(\epsilon^3) \quad (37)$$

where $|\epsilon| \ll 1$ and where $g(\mathbf{x}) = O(\epsilon^3)$. Now \mathbf{d} and \mathbf{e} cannot be freely chosen, as they are related by the condition

$$g(\mathbf{x}) - g(\mathbf{x}_0) = 0 = \epsilon \nabla g|_{\mathbf{x}_0} \cdot \mathbf{d} + \frac{1}{2} \epsilon^2 \nabla g|_{\mathbf{x}_0} \cdot \mathbf{e} + \frac{1}{2} \epsilon^2 \mathbf{d} \cdot \mathbf{G}_0 \cdot \mathbf{d} + O(\epsilon^3) \quad (38)$$

where $\mathbf{G} = \mathbf{G}(\mathbf{x})$ is the matrix with second derivative of g : $G_{ij} = \frac{\partial^2 g}{\partial x_i \partial x_j}$, and \mathbf{G}_0 means \mathbf{G} when evaluated on $\mathbf{x} = \mathbf{x}_0$. The Taylor expansion of V

to second order now writes:

$$V(\mathbf{x}) - V(\mathbf{x}_0) = \epsilon \nabla V|_{\mathbf{x}_0} \cdot \mathbf{d} + \frac{1}{2} \epsilon^2 \nabla V|_{\mathbf{x}_0} \cdot \mathbf{e} + \frac{1}{2} \epsilon^2 \mathbf{d} \cdot \mathbf{H}_0 \cdot \mathbf{d} + O(\epsilon^3) \quad (39)$$

Note that in the unconstrained case, the term involving \mathbf{e} vanishes because we had $\nabla V|_{\mathbf{x}_0} = 0$, but this is no longer the case here. Using (36), (38), and (39), the condition (33) writes:

$$V(\mathbf{x}) - V(\mathbf{x}_0) = \frac{1}{2} \epsilon^2 \mathbf{d} \cdot (\mathbf{H}_0 - \lambda \mathbf{G}_0) \cdot \mathbf{d} \geq 0 \quad \forall \mathbf{d} \text{ such that } \nabla g \cdot \mathbf{d} = 0 \quad (40)$$

We note $\hat{\mathbf{H}} := \mathbf{H} - \lambda \mathbf{G}$ the *augmented* Hessian matrix. As in the unconstrained case, a sufficient condition is obtained by requiring the matrix to be positive definite in the tangent plane of the surface $g = 0$ at point \mathbf{x}_0 (that is the \geq sign is replaced by a $>$ sign in (40)).

Example: We study the potential energy $V(x_1, x_2) = x_1^2 + x_2^2$ under the constraint $g(x_1, x_2) = (x_1 - 1)^2 + (x_2 - 2)^2 - 1 = 0$. Equilibrium are point A , such that $x_1^A = 1 - 1/\sqrt{5}$, $x_2^A = 2 - 2/\sqrt{5}$, $\lambda_A = 1 - \sqrt{5}$, and B , such that $x_1^B = 1 + 1/\sqrt{5}$, $x_2^B = 2 + 2/\sqrt{5}$, $\lambda_B = 1 + \sqrt{5}$. The augmented Hessian matrix is

$$\hat{\mathbf{H}}_A = \mathbf{H}_A - \lambda_A \mathbf{G}_A = \begin{pmatrix} +2\sqrt{5} & 0 \\ 0 & +2\sqrt{5} \end{pmatrix} \quad (41a)$$

$$\hat{\mathbf{H}}_B = \mathbf{H}_B - \lambda_B \mathbf{G}_B = \begin{pmatrix} -2\sqrt{5} & 0 \\ 0 & -2\sqrt{5} \end{pmatrix} \quad (41b)$$

We first note that this matrix is positive definite for point A and negative definite for point B . We now study them in the tangent plane of the surface $g = 0$ at points A and B . At point A , $\nabla V = -2/\sqrt{5}(1, 2)$. The perpendicular directions \mathbf{d} write $\alpha(-2, 1)$ with $\alpha \in \mathbb{R}$. Consequently $\mathbf{d} \cdot \hat{\mathbf{H}}_A \cdot \mathbf{d} = \alpha^2 10\sqrt{5} > 0$. Point A is a local minimum, a stable equilibrium. At point B , the perpendicular directions \mathbf{d} also write $\alpha(-2, 1)$ and $\mathbf{d} \cdot \hat{\mathbf{H}}_B \cdot \mathbf{d} = -\alpha^2 10\sqrt{5} > 0$. Point B is not a local minimum, it corresponds to an unstable equilibrium.

We note that the restriction $\nabla g \cdot \mathbf{d} = 0$ did not change anything to the result: in this example stability could have been correctly inferred from (41).

Example: We study the potential energy $V(x_1, x_2) = x_1^2 - x_2^2$ under the constraint $g(x_1, x_2) = x_2 + 1 = 0$. The equilibrium point is A with $x_1^A = 0$, $x_2^A = -1$, $\lambda_A = 2$. The augmented hessian matrix is:

$$\hat{\mathbf{H}}_A = \mathbf{H}_A - \lambda_A \mathbf{G}_A = \begin{pmatrix} 2 & 0 \\ 0 & -2 \end{pmatrix} \quad (42)$$

This matrix is not positive definite, as there is one negative eigenvalue. Nevertheless positive definitiveness has to be tested under the restriction $\nabla g \cdot \mathbf{d} = 0$. The perpendicular directions \mathbf{d} write $\alpha(1, 0)$ with $\alpha \in \mathbb{R}$. Consequently $\mathbf{d} \cdot \hat{\mathbf{H}}_A \cdot \mathbf{d} = 2\alpha^2 > 0$. Point A is then a local minimum, a stable equilibrium.

We note that the restriction $\nabla g \cdot \mathbf{d} = 0$ was important to consider, as without it we would have (incorrectly) concluded that A was an unstable equilibrium.

7.3 The projected Hessian matrix

In the case there are m equality constraints $g_j(\mathbf{x}) = 0$, with $j \in (1, m)$, we show how to verify that the augmented Hessian matrix $\hat{\mathbf{H}} = \mathbf{H} - \sum_j \lambda_j \mathbf{G}_j$ is positive definite in the tangent plane.

- We compute the gradients ∇g_j and place them as the lines of a matrix \mathbf{T} :

$$\mathbf{T} = \begin{pmatrix} - & \nabla g_1 & - \\ - & \nabla g_2 & - \\ - & \vdots & - \\ - & \nabla g_m & - \end{pmatrix} \quad (43)$$

- We compute the kernel of \mathbf{T} . Generically this yields a set of $(n - m)$ orthonormal vectors $\{k_1, k_2, \dots, k_{n-m}\}$ which span the tangent plane. We place these vectors in the lines of the matrix \mathbf{K} :

$$\mathbf{K} = \begin{pmatrix} - & \mathbf{k}_1 & - \\ - & \mathbf{k}_2 & - \\ - & \vdots & - \\ - & \mathbf{k}_{n-m} & - \end{pmatrix} \quad (44)$$

All possible vectors \mathbf{d} such that $\nabla g_j \cdot \mathbf{d} = 0 \forall j$ are generated with the help of the basis $\{\mathbf{k}_1, \mathbf{k}_2, \dots, \mathbf{k}_{n-m}\}$, that is we consider $\mathbf{d} = \alpha_1 \mathbf{k}_1 + \alpha_2 \mathbf{k}_2 + \dots + \alpha_{n-m} \mathbf{k}_{n-m}, \forall \alpha_j$. Writing $\mathbf{d}^* = (\alpha_1, \alpha_2, \dots, \alpha_{n-m})$, vectors \mathbf{d} are given by $\mathbf{d} = \mathbf{K}^T \cdot \mathbf{d}^*$.

- Consequently we want

$$\mathbf{d}^* \cdot \mathbf{K} \hat{\mathbf{H}} \mathbf{K}^T \cdot \mathbf{d}^* > 0 \quad \forall \mathbf{d}^* \quad (45)$$

We introduce $\hat{\mathbf{H}}^* := \mathbf{K} \hat{\mathbf{H}} \mathbf{K}^T$, the *projected* augmented Hessian matrix. This a square $(n - m) \times (n - m)$ symmetric matrix. Having only strictly positive eigenvalues implies stability. One (or more) negative eigenvalue yields instability. And in the case where all eigenvalues are positive but one

(or more) is zero, stability is undecided (computations at higher orders are needed).

Example: We study the potential energy $V(x_1, x_2, x_3) = x_1 + x_2^2 + x_2 x_3 + 2x_3^2$ under the constraint $g(x_1, x_2, x_3) = x_1^2 + x_2^2 + x_3^2 - 1 = 0$. One equilibrium point is A with $x_1^A = 1$, $x_2^A = 0$, $x_3^A = 0$, $\lambda_A = 1/2$. The augmented Hessian matrix is

$$\hat{\mathbf{H}}_A = \mathbf{H}_A - \lambda_A \mathbf{G}_A = \begin{pmatrix} -1 & 0 & 0 \\ 0 & 1 & 1 \\ 0 & 1 & 3 \end{pmatrix} \quad (46)$$

Eigenvalues are -1 , $2 - \sqrt{2}$, and $2 + \sqrt{2}$. The matrix $\mathbf{T}_A = (1, 0, 0)$ and finally

$$\mathbf{K}_A = \begin{pmatrix} 0 & 1 & 0 \\ 0 & 0 & 1 \end{pmatrix} \quad \text{and} \quad \hat{\mathbf{H}}_A^* = \begin{pmatrix} 1 & 1 \\ 1 & 3 \end{pmatrix} \quad (47)$$

The projected augmented Hessian matrix $\hat{\mathbf{H}}_A^*$ has eigenvalues $2 - \sqrt{2}$ and $2 + \sqrt{2}$, and consequently point A is a stable equilibrium.

Example: We minimize $V(x_1, x_2, x_3) = x_1^2 - x_2 + x_3^2$ under the two constraints $g_1(x_1, x_2, x_3) = x_1 + 2x_2 + x_3 - 1 = 0$ and $g_2(x_1, x_2, x_3) = 2x_1 - x_2 - 3x_3 - 4 = 0$. The equilibrium point is A with $x_1^A = 2/5$, $x_2^A = 1$, $x_3^A = -7/5$, $\lambda_1^A = -16/25$, and $\lambda_2^A = 18/25$. The Hessian matrix is:

$$\hat{\mathbf{H}}_A = \mathbf{H}_A - \lambda_A \mathbf{G}_A = \begin{pmatrix} 2 & 0 & 0 \\ 0 & -2 & 0 \\ 0 & 0 & 2 \end{pmatrix} \quad (48)$$

The matrix $\mathbf{T}_A = (1, 0, 0)$ and finally

$$\mathbf{T}_A = \begin{pmatrix} 1 & 2 & 1 \\ 2 & -1 & -3 \end{pmatrix} \quad \text{and} \quad \mathbf{K}_A = \begin{pmatrix} 1 & -1 & 1 \end{pmatrix} \quad \text{and} \quad \hat{\mathbf{H}}_A^* = 2 \quad (49)$$

Consequently point A is a local minimum.

7.4 Example: The aligned clamped beam

We here compute the buckling load of the two degrees of freedom system of Figure 7-Right. The potential energy of the system is

$$V = \frac{1}{2}k(\theta_1 - \theta_0)^2 + \frac{1}{2}k(\theta_2 - \theta_1)^2 + \frac{1}{2}k(\theta_3 - \theta_2)^2 + Ph(\cos \theta_0 + \cos \theta_1 + \cos \theta_2 + \cos \theta_3) \quad (50)$$

We introduce dimensionless variables $v = V/k$ and $p = 16Ph/k$ in order to follow notations of Equation (7). A first boundary condition implies that $\theta_0 = 0 = \theta_3$. The variables are then (θ_1, θ_2) . The second boundary condition implies a constraint $g(\theta_1, \theta_2) = \sin \theta_1 + \sin \theta_2 = 0$. Equilibrium equations are

$$2\theta_1 - \theta_2 - \frac{p}{16} \sin \theta_1 = \lambda \cos \theta_1 \quad (51a)$$

$$-\theta_1 + 2\theta_2 - \frac{p}{16} \sin \theta_2 = \lambda \cos \theta_2 \quad (51b)$$

$$\sin \theta_1 + \sin \theta_2 = 0 \quad (51c)$$

One trivial solution is $\theta_1 = 0 = \theta_2 = \lambda$. We study its stability. The augmented Hessian matrix is

$$\hat{\mathbf{H}}_0 = \begin{pmatrix} 2 - p/16 & -1 \\ -1 & 2 - p/16 \end{pmatrix} \quad (52)$$

The matrices $\mathbf{T} = (1, 1)$ and $\mathbf{K} = (-1, 1)$ yield the projected Hessian matrix $\hat{\mathbf{H}}_0^* = 6 - p/8$. The trivial solution is then stable for $p < 48$. This threshold $p = 48$ has to be compared with the threshold $p = 16$ found in Section 6.5: different boundary conditions yield different buckling loads.

8 Minimization with inequality constraints

Given a function $V(\mathbf{x})$, where $V \in \mathbb{R}$ and $\mathbf{x} \in \mathbb{R}^n$, we look for the point(s) for which V is locally minimum, but only for the point(s) that satisfy one (or more) constraints $f(\mathbf{x}) \geq 0$, see two examples in Figure 9.

Example: Minimize $V(x) = \frac{1}{4}x^4 - \frac{1}{3}x^3 - 2x^2 + 4x$ in the subset where $f(x) = x \geq 0$.

8.1 First derivative

We are given a function $V(\mathbf{x})$ that is to be minimized in the subset where $f(\mathbf{x}) \geq 0$. We require the point \mathbf{x}_0 to be a local minimum by stating that for small ϵ

$$V(\mathbf{x} = \mathbf{x}_0 + \epsilon \mathbf{d}) \geq V(\mathbf{x}_0) \quad \forall \mathbf{x} \text{ such that } f(\mathbf{x}_0 + \epsilon \mathbf{d}) \geq 0 \quad (53)$$

This means that not all \mathbf{d} directions will be tested. Only the directions \mathbf{d} fulfilling

$$f(\mathbf{x}_0 + \epsilon \mathbf{d}) = f(\mathbf{x}_0) + \epsilon \nabla f|_{\mathbf{x}_0} \cdot \mathbf{d} + O(\epsilon^2) \geq 0 \quad (54)$$

will be tested. There are two cases: (i) the point \mathbf{x}_0 is such that $f(\mathbf{x}_0) > 0$ (inactive constraint), or (ii) the point \mathbf{x}_0 is such that $f(\mathbf{x}_0) = 0$ (active constraint).

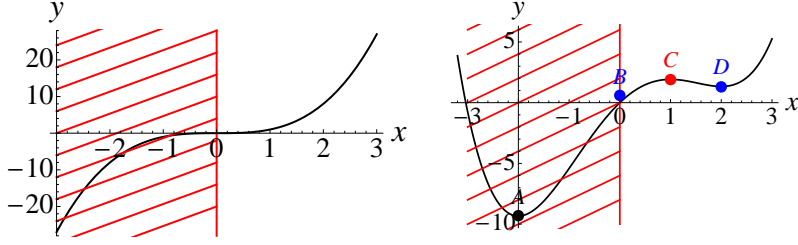


Figure 9. (Left) The function $V(x) = x^3$ with the constraint $x \geq 0$. (Right) The function $V(x) = \frac{1}{4}x^4 - \frac{1}{3}x^3 - 2x^2 + 4x$ with the constraint $x \geq 0$. Points B and D are local minima, point C is a local maximum, and point A is a forbidden minimum.

Inactive constraint ($f(\mathbf{x}_0) > 0$): In this case (54) is fulfilled for every direction \mathbf{d} . Consequently the first order necessary condition is the same as in the unconstrained case: $\nabla V|_{\mathbf{x}_0} = \mathbf{0}$, this is the case for points C and D in Figure 9-Right.

Active constraint ($f(\mathbf{x}_0) = 0$): Contrary to what was done in the case with equality constraints, the sign of ϵ and therefore the direction of $\epsilon\mathbf{d}$ cannot be arbitrary. Indeed, here (54) implies that $\nabla f|_{\mathbf{x}_0} \cdot \epsilon\mathbf{d}$ has to be positive. The first order condition is then

$$\nabla V|_{\mathbf{x}_0} \cdot \epsilon\mathbf{d} \geq 0 \quad \forall \mathbf{d} \text{ such that } \nabla f|_{\mathbf{x}_0} \cdot \epsilon\mathbf{d} \geq 0 \quad (55)$$

which implies that ∇V and ∇f are collinear and in the same direction, that is there is a real number μ such that

$$\nabla V|_{\mathbf{x}_0} = \mu \nabla f|_{\mathbf{x}_0} \text{ with } \mu \geq 0 \quad (56)$$

A way to write the first order condition in both the active and inactive cases is through the so-called Kuhn-Tucker conditions

$$\nabla V|_{\mathbf{x}_0} = \mu \nabla f|_{\mathbf{x}_0} \quad (57a)$$

$$\mu \geq 0 \quad (57b)$$

$$\mu f(\mathbf{x}_0) = 0 \quad (57c)$$

8.2 Second derivative

We consider the active and inactive constraint cases separately.

Inactive constraint ($f(\mathbf{x}_0) > 0$): as in the first order, every direction \mathbf{d} is to be considered and hence we obtain the same sufficient condition as in

the unconstrained case: $\mathbf{d} \cdot \mathbf{H}_0 \cdot \mathbf{d} > 0 \forall \mathbf{d}$. This condition is fulfilled by point D in Figure 9-Right.

For the active constraint case, we consider two sub-cases, (i) when the Lagrange multiplier $\mu > 0$ (strongly active constraint), and (ii) when the Lagrange multiplier $\mu = 0$ (weakly active constraint).

Strongly active constraint ($f(\mathbf{x}_0) = 0$ and $\mu > 0$): in this case the perturbations along the gradient of f (i.e. such that $\nabla f \cdot \mathbf{d} \neq 0$) are such that, to first order, $V(\mathbf{x}) - V(\mathbf{x}_0) = \nabla V \cdot \epsilon \mathbf{d} > 0$. Consequently we need only worry about the perturbations that let \mathbf{x} stay on the surface $f = 0$. As in the case with equality constraints, we develop the perturbation \mathbf{x} , $f(\mathbf{x})$, and $V(\mathbf{x})$ to second order, see (37)-(39). We obtain the necessary condition

$$V(\mathbf{x}) - V(\mathbf{x}_0) = \frac{1}{2}\epsilon^2 \mathbf{d} \cdot (\mathbf{H}_0 - \mu \mathbf{F}_0) \cdot \mathbf{d} \geq 0 \quad \forall \mathbf{d} \text{ such that } \nabla f \cdot \mathbf{d} = 0 \quad (58)$$

where $\mathbf{F} = \mathbf{F}(\mathbf{x})$ is the matrix with second derivative of f : $F_{ij} = \frac{\partial^2 f}{\partial x_i \partial x_j}$, and \mathbf{F}_0 means \mathbf{F} when evaluated on $\mathbf{x} = \mathbf{x}_0$. A sufficient condition is obtained by requiring the matrix $\mathbf{H}_0 - \mu \mathbf{F}_0$ to be positive definite in the tangent plane of the surface $f = 0$ at point \mathbf{x}_0 (that is the \geq sign is replaced by a $>$ sign in (58)).

Weakly active constraint ($f(\mathbf{x}_0) = 0$ and $\mu = 0$): in this case the first order of $V(\mathbf{x}) - V(\mathbf{x}_0)$ vanishes. As a sufficient condition we then ask that the second order $\mathbf{d} \cdot \mathbf{H}_0 \cdot \mathbf{d} > 0$ for all directions \mathbf{d} , including the direction along ∇f . This sufficient condition is not at all optimal, as can be seen in the example $V(x) = x^3$ with constraint $x \geq 0$ where the point $x = 0$ is clearly a local minimum even if the above sufficient condition is not fulfilled, see Figure 9-Left.

8.3 Summary

When studying the potential energy $V(\mathbf{x})$ subject to m inequality constraints $f_j(\mathbf{x}) \geq 0$ with $j \in (1, m)$, we first solve the set of nonlinear equations:

$$\mu_1 f_1(\mathbf{x}) = 0 \quad (59a)$$

$$\mu_2 f_2(\mathbf{x}) = 0 \quad (59b)$$

$$\vdots = 0$$

$$\mu_m f_m(\mathbf{x}) = 0 \quad (59c)$$

$$\nabla V(\mathbf{x}) - \sum_j \mu_j \nabla f_j(\mathbf{x}) = 0 \quad (59d)$$

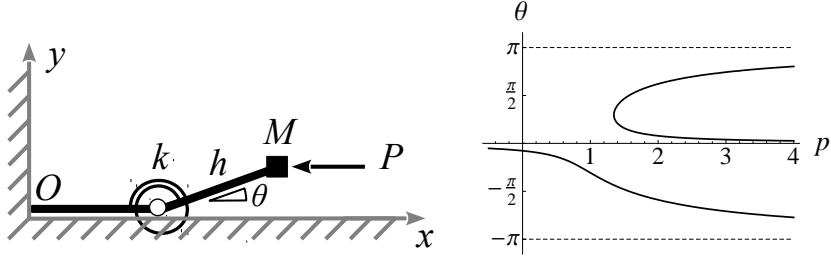


Figure 10. (Left) Two rigid bars linked by a spiral spring, with a punctual mass M at the extremity of the second bar. The system lies on a rigid support and is subject to an external compressive load P . (Right) Solution curves $\theta = \theta(p)$ of equation (62).

This yields a set of candidate local minima $\mathbf{x}_0 = \mathbf{x}_A, \mathbf{x}_B, \dots$ We review each candidate and eliminate those for which there is one (or more) j such that $f_j(\mathbf{x}_0) < 0$. Among the remaining candidates we eliminate those for which there is one (or more) j such that $\mu_j(\mathbf{x}_0) < 0$. For each remaining candidate, we build the projected Hessian matrix $\hat{\mathbf{H}}^* := \mathbf{K} \hat{\mathbf{H}} \mathbf{K}^T$ with $\hat{\mathbf{H}} = \mathbf{H} - \sum_j \mu_j \mathbf{F}_j$. The matrix \mathbf{K} is computed, as in Section 7.3, from the kernel of the matrix \mathbf{T} whose lines are the gradients ∇f_j for all j such that $\mu_j > 0$. We then compute the eigenvalues of $\hat{\mathbf{H}}^*$. If there is only strictly positive eigenvalues, the point \mathbf{x}_0 is a local minimum. But in the case where there is one (or more) zero or strictly negative eigenvalue, we cannot decide whether \mathbf{x}_0 is a local minimum or not. This shortcoming is due to the fact that when weakly active constraints are present, our sufficient condition is too demanding. As a matter of fact, if no weakly active constraint is present (that is $\mu_j > 0$ for all j such that $f_j(\mathbf{x}_0) = 0$) then stability is only undecided when zero eigenvalues are encountered, that is strictly negative eigenvalues yield instability.

8.4 Example: Buckling of heavy beam on rigid support

We study the equilibrium and stability of the system of Figure 10-Left, comprising two rigid bars of length h , linked by a spiral spring of stiffness k . The first bar is strongly anchored at the origin. At the extremity of the second bar lies a punctual mass M , and all the other components of the system are considered massless. An external horizontal force P is applied on the mass. The system is resting on a rigid, impenetrable support. To

the internal strain energy $\frac{1}{2}k\theta^2$ of the spiral spring we add the gravitational energy of the mass $M g h \sin \theta$ and the work of the external load $Ph(1+\cos \theta)$ to obtain the total potential energy V of the system. After division by k and subtraction of the constant $2Ph/k$, we obtain

$$v(\theta) = \frac{1}{2}\theta^2 + p(\cos \theta - 1) + m \sin \theta \quad (60)$$

where $v = V/k - 2Ph/k$, $p = Ph/k$, and $m = Mgh/k$. We study $v(\theta)$ under the constraint $y(M) \geq 0$, that is $f(\theta) = \sin \theta \geq 0$. We fix $m = 1/4$ and look for stable and unstable equilibrium solutions and their evolution as p is varied. We restrict to $p \in (0, 4)$ and $\theta \in (-\pi, \pi)$.

First order (equilibrium) equations are

$$v'(\theta) - \mu f'(\theta) = 0 \quad (61a)$$

$$\mu f(\theta) = 0 \quad (61b)$$

In the case where $\mu = 0$, (61a) is solved as

$$p = \frac{\theta + m \cos \theta}{\sin \theta} \quad (62)$$

and yields two distinct curves, see Figure 10-Right. The lower curve entirely lies in the region $f(\theta) < 0$ and is therefore discarded.

In the case where $f(\theta) = \sin \theta = 0$, we find that either (i) $\theta = 0$ with $m = \mu$, or (ii) $\theta = \pi$ with $\mu = m - \pi = 1/4 - \pi < 0$. This second solution with $\mu < 0$ is discarded.

We now turn to the stability test for the equilibrium we have just found.

In the case where $\mu = 0$, the constraint is passive ($f(\theta) > 0$) and consequently we need only test the second derivative $v''(\theta) = 1 - p \cos \theta - m \sin \theta$ for each point on the upper curve of Figure 10-Right. We find that stability changes at the fold point, see Section 9, and that the upper part (respectively the lower part) of the curve is stable (resp. unstable).

In the case where $f(\theta) = 0$, the equilibrium solution $\theta = 0$ has a strictly positive Lagrange multiplier $\mu = m > 0$ which is enough for stability in this one degree-of-freedom system.

The complete bifurcation curve, with stability information, is draw in Figure 11-Left. We remark that the trivial path $\theta = 0$ is stable for any load p and that it is not connected to the path of buckled states. We also remark that if the mass m is increased to $m > \pi$ a stable path $\theta = \pi$ appears for all p . Finally we see in Figure 11-Right that in this one degree-of-freedom problem equilibrium and their stability can readily be assessed by looking at the graph of $v(\theta)$ for different values of p .

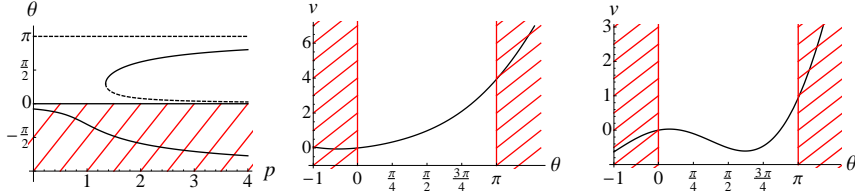


Figure 11. (Left) Complete bifurcation diagram for system of Figure 10-Left with $m = 1/4$, $p \in (0, 4)$, and $\theta \in (-\pi, \pi)$. Plain (respectively dashed) curves correspond to stable (resp. unstable) equilibria. (Center) The graph of $v(\theta)$ for $p = 0.5$ where the unique stable equilibrium is seen at $\theta = 0$. (Right) Same graph, yet for $p = 2$ where one additional unstable and one additional stable equilibria are present.

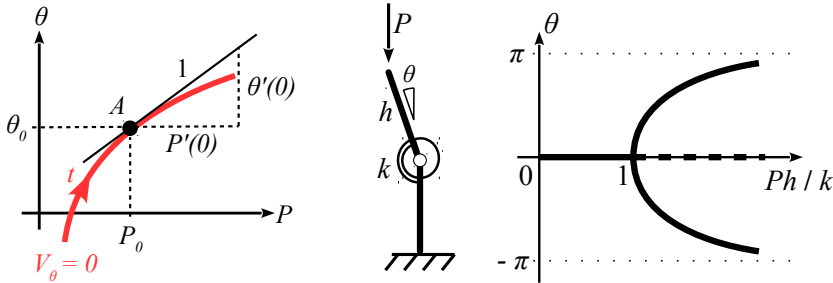


Figure 12. (Left) At point $A = (P_0, \theta_0)$, we look for the tangent approximation to the bifurcation curve $V_\theta(\theta, P) = 0$. (Right) One degree of freedom system and its bifurcation diagram.

9 Bifurcation diagrams

For simplicity reasons, in this section we treat the case of a one degree of freedom system, $V = V(\theta, P)$ where θ is the variable and P the applied load. Equilibrium are given by $V_\theta := \partial V / \partial \theta = 0$, and we want to plot the set of curve(s) implicitly defined by $V_\theta(\theta, P) = 0$ in the plane (P, θ) , see Figure 12. This set of curves is called the bifurcation diagram of the system. Treatments of the case with multiple degrees of freedom can be found for example in Iooss and Joseph (1989) or Nguyen (2000).

Example: The system of Figure 12-Right has energy $V(\theta, P) = \frac{1}{2}k\theta^2 + Ph\cos\theta$, its bifurcation diagram exhibits a pitchfork bifurcation point at $(Ph/k, \theta) = (1, 0)$.

We start at a known point on the bifurcation curve, $A = (P_0, \theta_0)$, and we use a parameter t to move about A . We approximate the parametric curve $(P(t), \theta(t))$ locally with the Taylor expansion

$$P(t) = P_0 + t P'(0) + O(t^2) \quad (63a)$$

$$\theta(t) = \theta_0 + t \theta'(0) + O(t^2) \quad (63b)$$

The goal is to find $P'(0)$ and $\theta'(0)$ in order to construct a tangent approximation to the curve at point A . By definition, point A satisfies $V_\theta(\theta_0, P_0) = 0$. The points in its neighborhood (63) along the bifurcation curve are also equilibrium points, hence they satisfy $V_\theta(\theta(t), P(t)) = 0$. We then have

$$V_\theta(\theta(t), P(t)) = 0 = V_\theta(\theta_0, P_0) + t P'(0) \left. \frac{\partial V_\theta}{\partial P} \right|_{t=0} + t \theta'(0) \left. \frac{\partial V_\theta}{\partial \theta} \right|_{t=0} + O(t^2) \quad (64)$$

We simply write $V_{\theta P} := \left. \frac{\partial V_\theta}{\partial P} \right|_{t=0}$ and $V_{\theta\theta} := \left. \frac{\partial V_\theta}{\partial \theta} \right|_{t=0}$ and we note that the latter is the Hessian at point A . At first order we have

$$P'(0) V_{\theta P} + \theta'(0) V_{\theta\theta} = 0 \quad (65)$$

As we are given both the potential energy V and point A , we know the second derivatives $V_{\theta P}$ and $V_{\theta\theta}$. Relation (65) is therefore an equation for the two unknowns $P'(0)$ and $\theta'(0)$. There are four cases, as illustrated in Figure 13:

- if $V_{\theta P} \neq 0$ and $V_{\theta\theta} \neq 0$ point A is a regular point of the bifurcation curve, which has local slope $\frac{d\theta}{dP} = -V_{\theta P}/V_{\theta\theta}$.
- if $V_{\theta P} = 0$ and $V_{\theta\theta} \neq 0$ point A is also a regular point. The bifurcation curve has an horizontal tangent at point A : $\frac{d\theta}{dP} = 0$.
- if $V_{\theta P} \neq 0$ and $V_{\theta\theta} = 0$ point A is a singular point. From (65), we see that $P'(0) = 0$ which mean that the curve $\theta = \theta(P)$ has a vertical tangent at point A . Such a point is called a limit point. Considering the bifurcation curve in the neighborhood of A , we see that the Hessian $V_{\theta\theta}$ generically changes sign at a limit point: instabilities arise at limit points.
- if $V_{\theta P} = 0$ and $V_{\theta\theta} = 0$ point A is a singular point. The first order expansion (64) entirely vanishes at such a point. Consequently we push (63) and (64) to second order and find

$$V_{\theta\theta\theta} \theta'(0)^2 + 2V_{\theta\theta P} P'(0) \theta'(0) + V_{\theta PP} P'(0)^2 = 0 \quad (66)$$

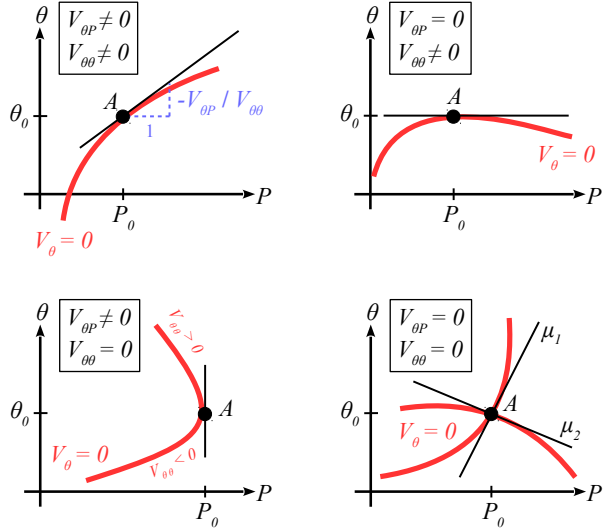


Figure 13. The four possible types of point along a bifurcation curve.

Generically this leads to two solutions for the tangent to the bifurcation curve, meaning that point A is a bifurcation point where two curves cross. From here there are two sub-cases:

- + if $V_{\theta\theta\theta} = 0$, then a first tangent is $P'(0) = 0$ (vertical tangent), and the second one is given by, provided $V_{\theta\theta P} \neq 0$, $\frac{d\theta}{dP} = -(1/2) V_{\theta PP}/V_{\theta\theta P}$.
- + if $V_{\theta\theta\theta} \neq 0$ then $P'(0) \neq 0$ and we can set $\mu := \theta'(0) = 0/P'(0) = 0$ and solve $V_{\theta\theta\theta} \mu^2 + 2V_{\theta\theta P} \mu + V_{\theta PP} = 0$. The two roots μ_1 and μ_2 have to be real, and provided they are distinct, we have the two tangents.

Here also the Hessian is going to change sign at the bifurcation point, instabilities arise at bifurcation points as well.

In conclusion we see that instabilities generically arise at singular points, limit or bifurcation points.

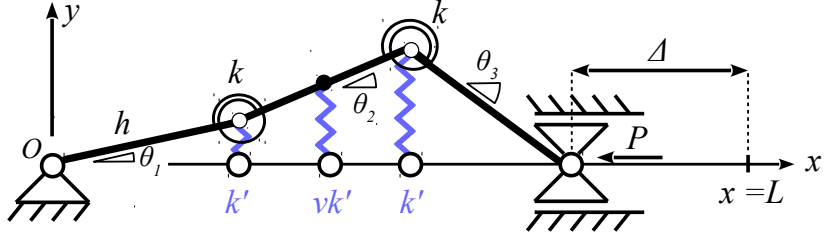


Figure 14. Stein's system: three rigid bars resting of a linear elastic foundation.

10 Buckling and post-buckling of a discrete beam on an elastic foundation

To illustrate the content of the previous sections, we treat the following example of a system of three rigid bars, see Figure 14. The bars have length h and therefore the system has a total contour length $L = 3h$. The three bars are linked together with two spiral springs of stiffness k , the first bar is held by a pivot fixed at the origin, and the third bar is held by a pivot that can slide along the horizontal axis. Moreover the second bar is tied to the ground with three linear springs of stiffness k' , $\nu k'$, and k' . These linear springs have zero rest length, and their foot are freely sliding along the horizontal axis. This model has been used by Stein (1959) to illustrate the rich behavior of stiffened elastic plates. Such a system has

$$V_{\text{int}} = \frac{1}{2}k(\theta_2 - \theta_1)^2 + \frac{1}{2}k(\theta_3 - \theta_2)^2 + \frac{1}{2}k'h^2 \sin^2 \theta_1 + \frac{1}{2}\nu k'h^2 (\sin \theta_1 + \frac{1}{2} \sin \theta_2)^2 + \frac{1}{2}k'h^2 \sin^2 \theta_3 \quad (67)$$

as internal energy. We choose $\nu = 2$. The work of the external load P is

$$V_{\text{ext}} = Ph (\cos \theta_1 + \cos \theta_2 + \cos \theta_3) \quad (68)$$

Boundary conditions impose a first constraint

$$g_1(\theta_1, \theta_2, \theta_3) = \sin \theta_1 + \sin \theta_2 + \sin \theta_3 = 0 \quad (69)$$

In the case of force-controlled loading the total potential energy is $V = V_{\text{int}} + V_{\text{ext}}$, while in the case of displacement-controlled loading it is simply

$V = V_{\text{int}}$. In the latter though, a second constraint is present

$$g_2(\theta_1, \theta_2, \theta_3) = h [\cos \theta_1 + \cos \theta_2 + \cos \theta_3] - (L - \Delta) = 0 \quad (70)$$

where Δ is the end-shortening, see Figure 14. We introduce dimension-

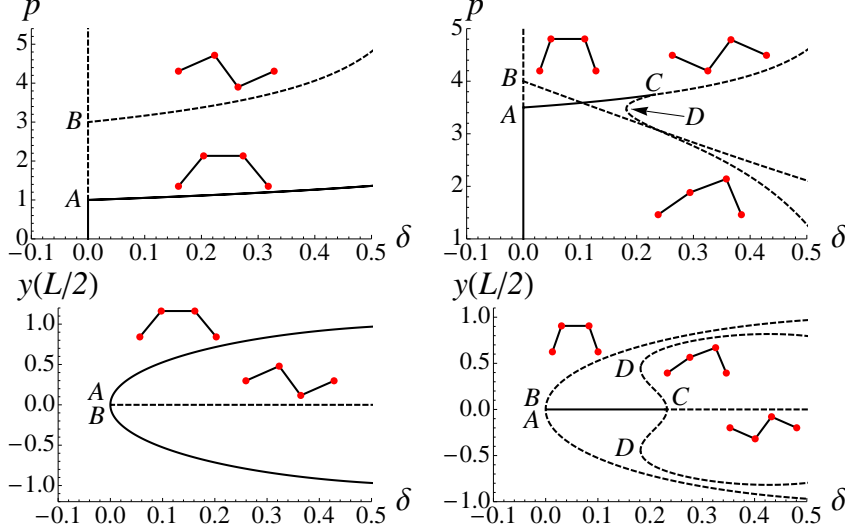


Figure 15. Bifurcation diagram for the system of Figure 14 in the force-controlled case. For both columns, we show two projections of the parameter space, namely (δ, p) for the upper diagram and $(\delta, y(L/2))$ for the lower diagram. Left column: without foundation, $\kappa = 0$. Right column: with foundation, $\kappa = 3/2$. Points A , B , C are pitchfork bifurcation points, and D is a fold point.

less quantities $v = V/k$, $\kappa = k' h^2/k$, $\delta = \Delta/(3h)$, and $p = Ph/k$. The augmented energy is then

$$\begin{aligned} v = & \frac{1}{2}(\theta_2 - \theta_1)^2 + \frac{1}{2}(\theta_3 - \theta_2)^2 + \frac{1}{2}\kappa \sin^2 \theta_1 + \frac{1}{2}\kappa (\sin \theta_1 + \frac{1}{2} \sin \theta_2)^2 \\ & + \frac{1}{2}\kappa (\sin \theta_3 + \frac{1}{2} \sin \theta_2)^2 + \frac{1}{2}\kappa \sin^2 \theta_3 \\ & + p [\cos \theta_1 + \cos \theta_2 + \cos \theta_3 - 3(1 - \delta)] - \lambda (\sin \theta_1 + \sin \theta_2 + \sin \theta_3) \end{aligned} \quad (71)$$

where, using (69), we have split the term corresponding to the extension of the center linear spring in two terms, rendering the energy symmetric with regards to the change $\theta_1 \leftrightarrow \theta_3$. We note λ the Lagrange multiplier associated to the constraint g_1 . In the case of force-controlled loading, p is the external force, while in the case of displacement-controlled loading it is the Lagrange multiplier associated to the constraint g_2 . We then see that the equilibrium equations $\partial v / \partial \theta_i = 0$, and consequently the equilibrium solutions, are the same for the two types of loading. Yet, computing the Hessian matrix, we see that stability depends on the loading type as the projected Hessian matrix is smaller in the case of the displacement-controlled loading: there are 3 variables $(\theta_1, \theta_2, \theta_3)$ and 1 constraint in the force-controlled case, generating a 2×2 projected Hessian matrix, while there are 2 constraints in the displacement-controlled case, generating a 1×1 projected Hessian matrix.

Writing the equilibrium equations $\partial v / \partial \theta_i = 0$, one sees that the straight configuration $(\theta_1, \theta_2, \theta_3) = (0, 0, 0)$ is solution $\forall p$. To test the stability of this trivial solution, we compute the Hessian matrix

$$\hat{\mathbf{H}}_0 = \begin{pmatrix} 1 + 2\kappa - p & -1 + \kappa/2 & 0 \\ -1 + \kappa/2 & 2 - p + \kappa/2 & -1 + \kappa/2 \\ 0 & -1 + \kappa/2 & 1 + 2\kappa - p \end{pmatrix} \quad (72)$$

We now restrict to the force-controlled case, and first focus on the case with no foundation, $\kappa = 0$. The augmented Hessian matrix has the three eigenvalues $\lambda_1 = -p$, $\lambda_2 = 1 - p$, and $\lambda_3 = 3 - p$, but to conclude on the stability the projected Hessian matrix has to be computed. The gradient of the constraint g_1 is evaluated at $(\theta_1, \theta_2, \theta_3) = (0, 0, 0)$ and written in the matrix $\mathbf{T} = (1, 1, 1)$. The null-space of \mathbf{T} is spanned by $\mathbf{k}_1 = (-1, 0, 1)/\sqrt{2}$ and $\mathbf{k}_2 = (-1, 2, -1)/\sqrt{6}$, leading to the matrix

$$\mathbf{K} = \begin{pmatrix} -1/\sqrt{2} & 0 & 1/\sqrt{2} \\ -1/\sqrt{6} & 2/\sqrt{6} & -1/\sqrt{6} \end{pmatrix} \text{ and } \hat{\mathbf{H}}_0^*(\kappa = 0) = \begin{pmatrix} 1 - p & 0 \\ 0 & 3 - p \end{pmatrix} \quad (73)$$

with $\hat{\mathbf{H}}^* := \mathbf{K} \hat{\mathbf{H}}_0 \mathbf{K}^T$. The straight solution becomes unstable as p reaches $p = 1$ where the system buckles into a symmetrical $\theta_1 = \theta_3$ shape, while at $p = 3$ a second (anti-symmetrical, $\theta_1 = -\theta_3$) buckling mode appears.

In the case $\kappa > 0$, the matrices \mathbf{T} and \mathbf{K} are the same, and the projected Hessian matrix is

$$\hat{\mathbf{H}}_0^*(\kappa) = \begin{pmatrix} 1 - p + 2\kappa & 0 \\ 0 & 3 - p + \kappa/3 \end{pmatrix} \quad (74)$$

We have here also two buckling modes $p_1 = 1 + 2\kappa$ and $p_2 = 3 + \kappa/3$, one symmetrical and the other anti-symmetrical. Depending on the κ value

(that is on the strength of the foundation) either the symmetrical or the anti-symmetrical one buckles first. Full bifurcation diagrams are shown in Figure 15 where we see that a non-symmetrical solution also exists. The branch containing these non-symmetrical solutions emanates from the secondary bifurcation point, labelled C . In the present force-controlled loading type, the branch comprises only unstable solutions, but in the case of displacement-controlled loading, the branch is stable after the fold point D .

11 Dynamical stability

Here, we generalize the previous concepts to discretized nonlinear elastic systems where dynamical effects cannot be longer neglected, see for example Guckenheimer and Holmes (1983) or Strogatz (1994). We will broaden our numerical tools not only to equilibrium states that are fixed in time but to periodic states that repeat in equal interval of time. Due to the complexity added by the presence of inertial terms, we will limit ourselves to minimization of mechanical energy without constraints.

Let's consider a one-degree-of-freedom system comprising two rigid bars of length L , as illustrated in Figure 16. The first bar is fixed on an infinitely rigid and massive base that eventually moves in a harmonic fashion following

$$y_a(t) = A \cos(\Omega t) \quad (75)$$

where A is the amplitude of the vertical oscillation and Ω is the frequency of the harmonic motion. The second bar is allowed to rotate at point B thanks to a viscoelastic hinge characterized by a rotating stiffness k and a viscous rotational damping c . The bars themselves are considered massless, and a concentrated mass M lies at the end of the second bar. The motion of the structure is parameterized by the angle $\theta(t)$ between the two bars. Such a system is a very simplified model for a heavy post fixed on an oscillating ground. The presence of harmonic excitations forces us to analyze the dynamics of the system.

11.1 Nonlinear equations of motion

We establish the equations of motion of the system of Figure 16. We first write down the kinetic energy of the system. The position of the material point M on the bar is expressed as a function of $\theta(t)$ at every time t in the Cartesian frame (O, x, y) :

$$\mathbf{OM}(t) = \left\{ \begin{array}{l} x_a - L \sin \theta(t) \\ y_a(t) + L + L \cos \theta(t) \end{array} \right\} \quad (76)$$

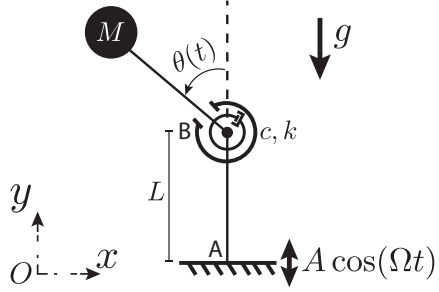


Figure 16. An initially vertical articulated system of two rigid bars, each of length L , supporting a concentrated mass M . The articulation is characterized by a rotational stiffness, k , and a viscous rotational damping, c . The structure is fixed at its base. The base vibrates in a harmonic fashion with an amplitude A and a frequency Ω . At each time t , the position of the moving bar in the $2D$ plane is parameterized by the angle $\theta(t)$ of the second bar with the vertical y -axis.

where x_a is fixed and $y_a(t)$ is given by (75). The velocity of the material point of mass M is therefore

$$\mathbf{v}(t) = \mathbf{O}\dot{\mathbf{M}}(t) = \begin{Bmatrix} -L\dot{\theta} \cos \theta \\ -A\Omega \sin(\Omega t) - L\dot{\theta} \sin \theta \end{Bmatrix} \quad (77)$$

The kinetic energy then reads

$$T = \frac{1}{2}M\mathbf{v}^2(t) = \frac{1}{2}M \left[L^2\dot{\theta}^2 + A^2\Omega^2 \sin^2(\Omega t) + 2AL\Omega\dot{\theta} \sin(\Omega t) \sin \theta \right] \quad (78)$$

Virtual power of the external torques The virtual power of the reaction torque due to the stiffness of the circular spring simply writes

$$P_{ek} = -k\theta \delta\dot{\theta} \quad (79)$$

where $\delta\dot{\theta}$ is the virtual angular velocity carrying the velocity $\dot{\theta}$. The virtual power of the reaction torque due to the viscous damper reads

$$P_{ec} = -c\dot{\theta} \delta\dot{\theta} \quad (80)$$

The virtual power of the external torque due to the weight of the concentrated mass, $\mathbf{P} = -Mg\mathbf{e}_y$, is calculated considering the power moment of \mathbf{P} at point B in the virtual angular velocity $\delta\dot{\theta}$

$$P_{eM} = (\mathbf{BM} \times \mathbf{P}) \cdot \delta\dot{\theta} \mathbf{e}_z = MgL \delta\dot{\theta} \sin \theta \quad (81)$$

Note that the spring reaction torque and the torque of external force are conservative torques that derive from the potential energy

$$V = \frac{1}{2}k\theta^2 + MgL \cos \theta. \quad (82)$$

Lagrange formalism From the kinetic energy of the system, Eq. (78), we calculate the virtual power of the quantity of acceleration through Lagrange formula:

$$A_q = \left[\frac{d}{dt} \left(\frac{\partial T}{\partial \dot{q}_i} \right) - \frac{\partial T}{\partial q_i} \right] \delta \dot{q}_i \quad (83)$$

where the q_i are the generalized coordinates. The principle of virtual power, $A_q = P_{ek} + P_{ec} + P_{eM}$, yields the equation of motion of our discrete system

$$\frac{\partial}{\partial t} \left(\frac{\partial T}{\partial \dot{q}_i} \right) - \frac{\partial T}{\partial q_i} + \frac{\partial V}{\partial q_i} = Q_i \quad (84)$$

where Q_i is obtained from the virtual power of the non conservative external forces such that $P_{ec} = Q_i \delta \dot{q}_i$. We apply Eq. (84) to our system and obtain the nonlinear equation of motion for $q_1(t) = \theta(t)$

$$\ddot{\theta} + \frac{c}{ML^2} \dot{\theta} + \frac{k}{ML^2} \theta + \left(\frac{A\Omega^2}{L} \cos(\Omega t) - \frac{g}{L} \right) \sin \theta = 0 \quad (85)$$

We introduce the dimensionless variables $\tau = (\Omega/2)t$ and multiply (85) by $4/\Omega^2$ to rewrite it in dimensionless form

$$\ddot{\theta} + \frac{2}{\beta Q} \dot{\theta} + \frac{4}{\beta^2} \theta + \left(2\varepsilon \cos(2\tau) - \frac{4}{\beta^2} p \right) \sin \theta = 0 \quad (86)$$

where (\cdot) denotes differentiation with respect to τ , $Q = \frac{\sqrt{kML^2}}{c}$ is the quality factor, $\beta = \Omega/\Omega_0$ is the ratio between the excitation and a pseudo natural frequency $\Omega_0 = \sqrt{k/(ML^2)}$, $\varepsilon = 2A/L$ is the dimensionless amplitude of the harmonic motion of the base, and $p = MgL/k$ is a crucial dimensionless loading parameter for the static problem modeling the ratio between weight and stiffness of the system.

For convenience, we write this second order nonlinear ordinary differential equation as a two dimensional dynamical system $\dot{\mathbf{x}} = \mathbf{f}(\mathbf{x}, \tau)$:

$$\begin{cases} \dot{\theta} = \phi \\ \dot{\phi} = -\frac{2}{\beta Q} \phi - \frac{4}{\beta^2} \theta - \left(2\varepsilon \cos(2\tau) - \frac{4}{\beta^2} p \right) \sin \theta \end{cases} \quad (87)$$

where $\mathbf{x}(\tau) = \{\theta(\tau), \phi(\tau)\}^T$ is the 2-dimensional state vector and $\mathbf{f}(\mathbf{x}, \tau)$ is a nonlinear 2-dimensional vector field.

11.2 Particular case of a standstill base ($\varepsilon = 0$)

In this section we consider the case where the base is not in motion, that is we set $\varepsilon = 0$. We further fix $\beta = 1$ with no loss of generality. The equations of motion take the form $\dot{\mathbf{x}} = \mathbf{f}_1(\mathbf{x}, \tau)$, that is

$$\begin{cases} \dot{\theta} = \phi \\ \dot{\phi} = -\frac{2}{Q}\phi - 4\theta + 4p \sin \theta \end{cases} \quad (88)$$

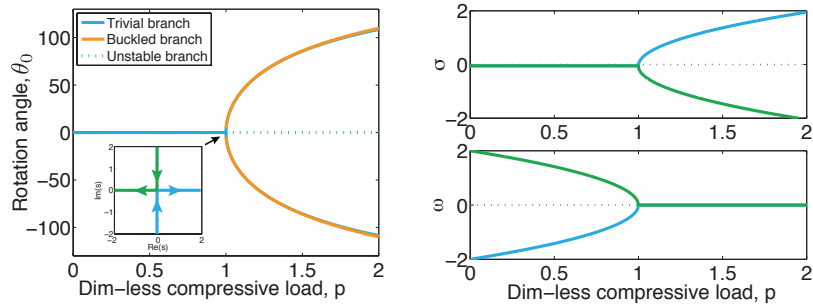


Figure 17. Branches of equilibrium solutions and linear stability analysis. (Left) Bifurcation diagram from the equilibria of system (88): equilibrium angle θ_0 as function of the dimensionless loading parameter p . Inset: Evolution in the Argand plane of the eigenvalues of the associated linearized dynamical equations around the trivial equilibrium point. (Right) Evolution of growth rate σ and frequency ω of the fundamental solutions $\mathbf{y}(\tau)$ of Eq. (90) as a function of p .

Bifurcation diagram and stability of equilibrium Equilibrium solutions are defined as solutions to Eq. (88) with $\dot{\phi} = 0 = \dot{\theta}$. We therefore have $\mathbf{x}(\tau) = \mathbf{x}_0 = \{\theta_0, 0\}^T$ and the equilibrium angle θ_0 solution of

$$\theta_0 - p \sin \theta_0 = 0. \quad (89)$$

For $p \in (0, 2)$, the nonlinear solution to (89) comprises two branches, see Figure 17-Left. The trivial branch is simply $\theta_0 = 0$, i.e. $\mathbf{x}_0 = \{0, 0\}^T = \mathbf{0}$. To assess the stability of this trivial equilibrium, we study the behavior of Eq. (88) for small $\theta(\tau)$ and $\phi(\tau)$, that is we set $\theta(\tau) = \theta_0 + \theta^*(\tau)$ and $\phi(\tau) = \phi^*(\tau)$ where $\theta^*(\tau)$ and $\phi^*(\tau)$ are small, and $\theta_0 = 0$. Injecting this in Eq. (88) and linearizing to first order, we obtain the so-called linearized equations of motion in the state space

$$\dot{\mathbf{y}}(\tau) = \mathbf{J}_1 \mathbf{y}(\tau) \quad (90)$$

$$\text{with } \mathbf{y}(\tau) = \begin{Bmatrix} \theta^*(\tau) \\ \phi^*(\tau) \end{Bmatrix} \quad \text{and} \quad \mathbf{J}_1 = \frac{\partial \mathbf{f}_1}{\partial \mathbf{x}} \Big|_{\mathbf{0}} = \begin{bmatrix} 0 & 1 \\ (4\lambda - 4) & -\frac{2}{Q} \end{bmatrix}$$

where $\mathbf{J}_1(\mathbf{x}_0, \lambda)$ is the Jacobi matrix of the nonlinear vector field $\mathbf{f}_1(\mathbf{x}, \tau)$, given in Eq. (88), evaluated at the trivial equilibrium point $\mathbf{x}_0 = \mathbf{0}$. The linear stability of this point is assessed by analyzing the perturbation vector $\mathbf{y}(\tau)$ when assuming a perturbation of the form

$$\mathbf{y}(\tau) = \mathbf{r} e^{s\tau} \quad \text{with} \quad \mathbf{r} = r \begin{Bmatrix} 1 \\ s \end{Bmatrix} \quad (91)$$

where the exponents $s = \sigma + i\omega$ can be complex numbers with σ , the growth rate or Lyapunov exponent and ω , the dimensionless frequency of the pseudo-harmonic eigenmode \mathbf{r} . Injecting $\mathbf{y}(\tau)$ in Eq. (90), we obtain the eigenvalue problem

$$[\mathbf{J}_1 - s\mathbf{1}] \mathbf{r} = \mathbf{0} \quad (92)$$

where $\mathbf{1}$ is the 2×2 identity matrix. Since the dimension of this eigenvalue problem in the state space is $N = 2$, i.e. twice the number of degree of freedom, Eq.(92) yields 2 eigenmodes \mathbf{r}_n and 2 eigenvalues s_n . The evolution of the real, $\Re(s)$, and imaginary, $\Im(s)$, parts of the eigenvalues s_n of the linearized problem Eq. (90) as function of the loading parameter p is drawn in Figure 17-Right. The linear stability of the considered equilibrium

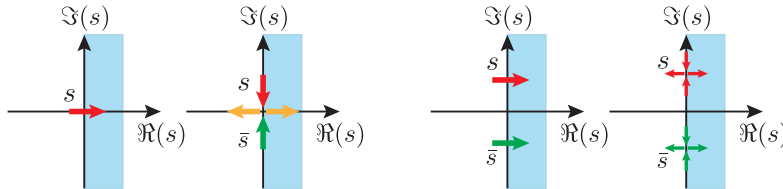


Figure 18. Stability of an equilibrium in the Argand plane. (Left) Static instability or instability by divergence can happen by simple crossing or locking of eigenvalues on the real axis. (Right) Dynamic instability or flutter instability can happen by crossing or locking of eigenvalues away from the real axis.

θ_0 is assessed by analyzing the eigenvalues s_n , i.e. the spectrum of the harmonic eigenmodes $\mathbf{y}_n(\tau)$ given by Eq. (91). According to Lyapunov theory, here are the following fundamental results when dealing with autonomous dynamical systems such as the one described in Eq. (88):

- If $\Re(s_n) < 0$ for all n , the equilibrium is asymptotically stable.

- If $\Re(s_n) \leq 0$ for all n and there is at least one index k such that $\Re(s_k) = 0$, one cannot conclude with a linearized stability analysis. Higher order considerations are needed.
- If amongst all the eigenvalues there exists one index k such that $\Re(s_k) > 0$, the equilibrium is unstable but two different scenarios have to be considered:
 - If $\Im(s_k) = 0$, the perturbed motion dramatically grows along the direction of the k^{th} mode \mathbf{r}_k in an exponential way. This loss of stability is called an instability by divergence or a static instability (buckling presented in the previous sections is such an instability). In the Argand plane, there are two scenarios for such an instability (see Figure 18-Left): *i*) one purely real eigenvalue crosses the imaginary axis, or *ii*) the imaginary parts of two conjugate eigenvalues annihilate to form one purely real eigenvalue crossing the imaginary axis.
 - If $\Im(s_k) \neq 0$, the perturbed motion is an harmonic oscillation that exponentially grows in the direction of the k^{th} mode \mathbf{r}_k . This loss of stability is referred to as a flutter instability or more generally as a dynamic instability. The representation in the Argand plane of such instabilities is illustrated in Figure 18-Right where two scenarios have to be considered: *i*) the crossing of the imaginary axis by two conjugate eigenvalues, or *ii*) the locking of two physical eigenvalues that causes the real part of one of them to cross the imaginary axis. The dynamic instability is an indicator of a Hopf bifurcation. In this kind of bifurcation, not only the dynamical system qualitatively bifurcates in the state space but also in the time domain, i.e. the equilibrium bifurcates to a periodic state (limit cycle).

In Figure 17-Right, we represent the evolution of the real and imaginary part of the two eigenvalues s_1 and s_2 of the eigenvalue problem Eq. (92) as function of the loading parameter p when $Q = 20$ (subcritical damping). These curves inform us about the linear stability of the trivial equilibrium branch $\theta_0 = 0$. As expected, above the critical load, $p > 1$, the thermodynamic branch becomes statically unstable and the straight equilibrium configuration $\theta_0 = 0$ is no longer a physical configuration for our articulated system. The inset of Figure 17-Left is the representation of the evolution of eigenvalues s_i in the Argand plane. As illustrated in Figure 18-Left, the system loses stability by the meeting of two purely imaginary and conjugate eigenvalues, which is a particular case of instability by divergence. Above the critical load, $p > 1$, the articulated bar buckles and possible equilibrium solutions with $\theta_0 \neq 0$ exist. To compute those stable bifurcated branches, one

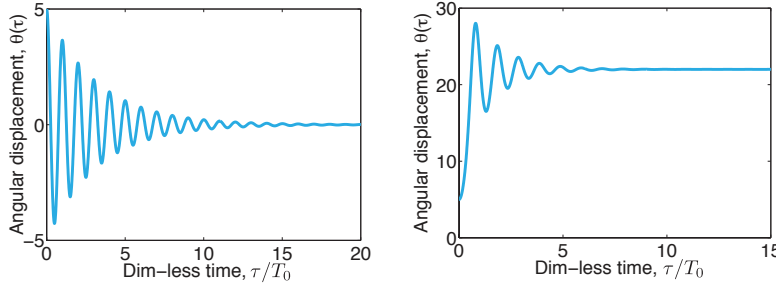


Figure 19. Temporal evolutions $\theta(\tau)$ as a function of dimensionless time τ/T_0 for initial conditions $\mathbf{x}(0) = \{5^\circ, 0\}^T$ and $Q = 20$. (Left) For $p = 0.75$. (Right) For $p = 1.025$.

needs to solve the nonlinear algebraic equation given in Eq. (89). Here, we simply perform a Taylor expansion of the sine function and Eq.(89) becomes

$$\theta_0 - p \left(\theta_0 - \frac{\theta_0^3}{6} + \frac{\theta_0^5}{120} - \dots \right) = 0. \quad (93)$$

Truncating the series (93) up to the fifth order, we obtain a fourth order polynomial equation with analytical solutions depending on the loading parameter p :

$$\theta_{\pm} = \sqrt{10 \pm \sqrt{\frac{20(6-p)}{p}}} \quad (94)$$

The solution θ_- is a local minimum of the potential energy and is represented in the bifurcation diagram of Figure 17-Left (we represent also the solution $-\theta_-$, the bifurcation being symmetric). We also compare the approximated solution θ_- with the one obtained by solving Eq. (89) with a classic Newton-Raphson algorithm. As the curves are barely distinguishable, we conclude that a fifth order approximation on the sine function is sufficient to correctly capture the mechanical behavior, up to a loading parameter $p = 2$. Note that the solution θ_+ is associated with a higher potential energy and corresponds to an unstable equilibrium configuration where the articulated rigid bar is rotated by more than a turn. As this solution disappears when the order of the series (93) is changed, we do not consider this ‘spurious’ solution here, see Domokos and Holmes (1993).

Direct dynamic analysis We recover the qualitative static behavior previously discussed by directly solving the nonlinear system of ordinary dif-

ferential equations given in Eq. (88) for various initial conditions $\mathbf{x}(0) = \{\theta(0), \phi(0)\}^T$. In Figure 19, we represent the evolution of $\theta(\tau)$ as a function of dimensionless time τ/T_0 , with $T_0 = 2\pi/\sqrt{4(1-p\cos\theta_0)}$ the period of the small amplitude oscillations around the stable equilibrium $\theta_0(p)$. We set the quality factor to $Q = 20$, use the initial condition $\mathbf{x}(0) = \{5^\circ, 0\}^T$, and plot the evolution of $\theta(\tau)$ for $p = 0.75$ in Figure 19-Left and $p = 1.025$ in Figure 19-Right. For $p = 0.75$, a loading parameter below the critical value $p = 1$, the initially perturbed articulated rigid bar undergoes damped oscillations until it eventually converges to the stable equilibrium position $\theta_0 = 0$. When choosing $p = 1.025 > 1$, the motion diverges from its initial position before performing exponentially decreasing oscillations around the equilibrium $\theta \simeq \theta_-$, see Eq. (94). Another representation of the dynam-

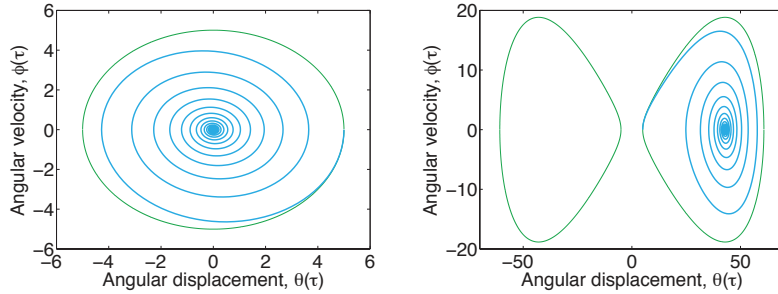


Figure 20. Dynamical response of Figure 19 in the phase plane $(\theta(\tau), \phi(\tau))$. (Left) Trajectory for $p = 0.75$ and $\mathbf{x}(0) = \{5^\circ, 0\}^T$. (Right) Trajectories for $p = 1.025$ and $\mathbf{x}(0) = \{5^\circ, 0\}^T$ or $\mathbf{x}(0) = \{-5^\circ, 0\}^T$.

ical behavior of our articulated system is to draw the phase portrait. In Figure 20-Left and 20-Right, we represent respectively the dynamical response of Figure 19-Left and 19-Right in the phase plane $(\theta(\tau), \phi(\tau))$. We see that the trajectory spirals down to $\mathbf{x}(\tau) = \{0, 0\}^T$ when $p < 1$, and to $\{\theta \simeq \theta_-, 0\}^T$ or $\{\theta \simeq -\theta_-, 0\}^T$ for $p > 1$ (whether the trajectory converges to the left or right side of the θ -axis is determined by the initial conditions).

In the absence of dissipation, $Q \rightarrow +\infty$ in Eq. (88), the system becomes conservative. The total mechanical E energy is the sum of kinetic, T , and potential energy, V , reads

$$E(\theta, \phi) = T(\phi) + V(\theta) = \frac{1}{2}\phi^2 + \frac{1}{2}4\theta^2 + 4p\cos\theta \quad (95)$$

As $\dot{E} = 0$, the trajectory of a solution in the phase plane of this conservative system is the level curve $E(\theta, \phi) = E_0$ with E_0 determined by the initial

condition $\{\theta(0), \phi(0)\}^T$. From Eq. (95), we write

$$\phi = \pm \sqrt{2(E_0 - V(\theta))} \quad (96)$$

and we plot in Figure 20, in green, the trajectories given by (96) for $\mathbf{x}(0) = \{5^\circ, 0\}^T$. These trajectories correspond to the motion the articulated bar would have if it was undamped.

11.3 General case of a moving base ($\varepsilon > 0$)

In the general case of a base moving with a harmonic motion $y_a(t) = A \cos(\Omega t)$, the dynamic response of the articulated rigid bar, $\theta(\tau)$, is determined by Eq. (87). This equation of motion is more complicated than in the previous section since Eq. (87) is a nonlinear ordinary differential equation with a periodic coefficient: the term $2\varepsilon \cos(2\tau)$ with a period $T = \pi$. This type of equation often arises in structural dynamics, notably every time we are interested in characterizing the small oscillations of a structure which is itself in a periodic state, see Bolotin (1964). Here, we are looking for the transverse oscillations of an articulated system resting on a moving foundation. This type of system is called a parametric oscillator, i.e. an oscillator (case of the previous subsection) whose geometrical or mechanical parameters periodically oscillate in time. In our case, it is the quantity of acceleration, A_q , given in Eq. (83), that is changing with time.

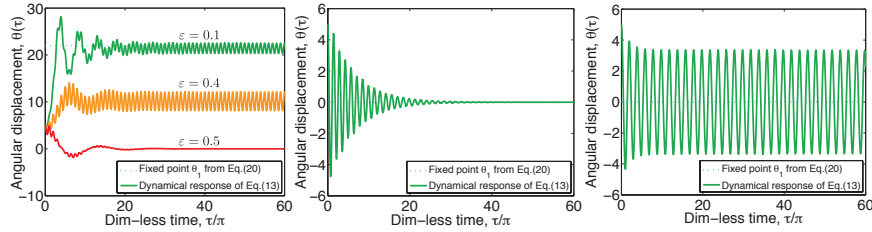


Figure 21. Temporal evolutions for $\theta(\tau)$, solution of Eq. (87), for initial conditions $\mathbf{x}(0) = \{5^\circ, 0\}^T$, $Q = 20$ and $\beta = 1$. (Left) Dynamical response for $p = 1.025$ (that is $\delta = -0.1$) and various $\varepsilon = [0.1, 0.4, 0.5]$. (Center) Dynamical response for $p = 0.5$ (that is $\delta = 2$) and $\varepsilon = 0.1$. (Right) Dynamical response for $p = 0.75$ (that is $\delta = 1$) and $\varepsilon = 0.1$.

Direct dynamic analysis To emphasize the complexity of this parametric oscillator, we perform direct computations of Eq. (87) with the operator

ode45 of the Matlab software for initial conditions, $\mathbf{x}(0) = \{5^\circ, 0\}^T$, a quality factor $Q = 20$, and a frequency ratio fixed to $\beta = \Omega/\Omega_0 = 1$. The temporal evolution $\theta(\tau)$ as a function of dimensionless time τ/π , with π the dimensionless period of the moving foundation, is given in Figure 21 for different values of the loading parameter p and amplitude of the forcing ε .

In Figure 21-Left, we show results for $p = 1.025$, just above the critical buckling threshold $p = 1$. We have seen in the previous section, Figure 19-Right and Figure 20-Right, that for $\varepsilon = 0$ the dynamical response $\theta(\tau)$ diverges from the unstable trivial equilibrium $\theta_0 = 0$ and settle on the bifurcated equilibrium $\theta_0 \simeq \theta_- = 22^\circ$ in an exponentially damped oscillatory fashion. For small $\varepsilon = 0.1$, we see on Figure 21-Left that the dynamical response of our parametric oscillator also diverges from the unstable configuration $\theta_0 = 0$, but now the solution $\theta(\tau)$ settle to stationary oscillations of period π near the value $\theta_0 \simeq \theta_- = 22^\circ$. This stable limit cycle appears because the moving base is acting as an external harmonic excitation of period π . When increasing ε , the dynamical response still diverges from $\theta_0 = 0$ to converge to a π -periodic limit cycle with larger amplitude, but the mean value of the oscillations becomes closer to $\theta = 0$ as ε increases. Surprisingly, above $\varepsilon \simeq 0.5$, i.e. an amplitude of forcing of the base $A = L/4$, the dynamic response is qualitatively different. The motion of the base stabilizes the equilibrium point $\theta_0 = 0$ and the parametric oscillations asymptotically converge to the straight vertical position.

In Figure 21-Center and 21-Right, we show results for p values below the critical buckling threshold. The amplitude of the forcing is set to $\varepsilon = 0.1$. For $p = 0.5$ the dynamic response, shown in Figure 21-Center, is qualitatively similar to the case with no forcing (see Figure 19-Left): The initially perturbed system undergoes damped oscillations until it eventually exponentially converges to the stable equilibrium position $\theta_0 = 0$. For $p = 0.75$, Figure 21-Right, the temporal evolution $\theta(\tau)$ is qualitatively different from Figure 19-Left and Figure 20-Left: The initially perturbed solution rapidly converges to a limit cycle with oscillations centered around the equilibrium configuration $\theta_0 = 0$, even if we are below the critical buckling threshold. Note that the dynamical response has a period 2π which is twice slower than the motion of the base (we have almost exactly 30 oscillations in 60 periods of the moving base). This phenomenon of self-sustaining oscillations is the well-known parametric instability. For example, a well known parametric instability is a child pumping a swing by periodically standing and squatting to increase the amplitude of the swing's oscillations.

Linear stability analysis In the case of periodic forcing when the base oscillates up and down, the equilibrium solution $\mathbf{x}_0 = \mathbf{0}$ nevertheless exists

and corresponds to the system being straight and oscillating vertically with the base. We now perform a linear stability analysis of this vertical equilibrium solution to get a better understanding of the physics of the periodic trivial state. We consider the non-autonomous 2-dimensional dynamical systems, Eq. (87), $\dot{\mathbf{x}}(\tau) = \mathbf{f}(\mathbf{x}(\tau), \tau, p)$ where \mathbf{f} is a nonlinear 2-dimensional vector field that intrinsically depends on the time τ . The stability of the oscillating vertical equilibrium configuration is studied by considering the dynamics of $\mathbf{x}(\tau) = \mathbf{x}_0 + \mathbf{y}(\tau)$ where $\mathbf{y}(\tau)$ is a small disturbance to the equilibrium \mathbf{x}_0 . Injecting $\mathbf{x}(\tau)$ into (87), assuming that \mathbf{f} is at least twice continuously differentiable, expanding the result in a Taylor series about \mathbf{x}_0 , and retaining only linear terms in the disturbance, we obtain

$$\dot{\mathbf{y}}(\tau) = \mathbf{J}(\tau)\mathbf{y}(\tau) \quad (97)$$

$$\text{with } \mathbf{J}(\tau) = \frac{\partial \mathbf{f}}{\partial \mathbf{x}} \Big|_{\mathbf{x}_0} = \begin{bmatrix} 0 & 1 \\ -(\delta + 2\varepsilon \cos 2\tau) & -\frac{2}{\beta Q} \end{bmatrix}$$

and where $\delta = 4(1-p)/\beta^2$ is the ratio between the natural frequency ω_0 of the articulated bar with the concentrated mass M and the frequency of the moving base, Ω . We have $\omega_0 = \sqrt{k/(ML^2) - g/L}$ and hence $\delta = 4\omega_0^2/\Omega^2$. As in the previous section $\mathbf{J}(\tau)$ is the 2×2 Jacobi matrix of \mathbf{f} , evaluated at $\mathbf{x}(\tau) = \mathbf{x}_0 = \mathbf{0}$. The linear system Eq.(97) is a generalization of the autonomous system Eq.(90) with $\varepsilon \neq 0$. The particular form Eq. (97) is called the Mathieu equation. It is more common to express it in the physical space, as a linearization of Eq. (86) about the solution $\theta(\tau) = 0$. It then reads

$$\ddot{\theta}(\tau) + \frac{2}{\beta Q} \dot{\theta}(\tau) + [\delta + 2\varepsilon \cos 2\tau] \theta(\tau) = 0 \quad (98)$$

Here the two parameters of interest are on one hand δ , the ratio between the natural frequency of the system and the frequency of the moving base, and on the other hand ε , the dimensionless amplitude of the forcing from the base. Note that for practical purposes δ is tuned either through the compressive loading parameter p , or through the frequency of the moving base Ω .

The linear stability study of the vertical configuration in periodic state consists in computing the solutions of Eq. (97) and determining whether the disturbance $\mathbf{y}(\tau)$ fades away or is amplified with time τ . The difficulty though, as compared to the previous section, is that the system Eq. (97) is a linear system *with periodic coefficients* since $\mathbf{J}(\tau)$ is π -periodic in time due to the presence of the forcing term $2\varepsilon \cos 2\tau$. The theoretical tools introduced in the previous subsection are therefore no longer applicable. To compute the solutions $\mathbf{y}(\tau)$ of linear equations such as the Mathieu

equation, we follow the theory introduced by Gaston Floquet at the end of the 19th century which deals with ordinary differential equations with periodic coefficients.

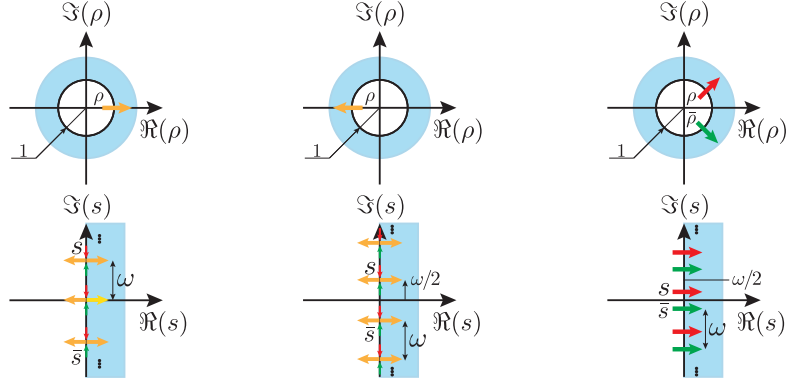


Figure 22. Stability of a periodic state, or limit cycle, in the Argand plane through Floquet multipliers (top row) or Floquet exponents (bottom row). (Left) Steady bifurcation: one purely real Floquet multiplier crosses the unit circle from the right in the time domain or Floquet exponents locked on a multiple of ω in the frequency domain. (Center) Flip or period-doubling bifurcation: one purely real Floquet multiplier crosses the unit circle from the left or Floquet exponents locked on a multiple of $\omega/2$. (Right) Secondary Hopf, or Neimark-Sacker bifurcation: two conjugate Floquet multipliers cross the unit circle at away from the real axis or Floquet exponents cross the imaginary axis at values different from a multiple of $\omega/2$.

Floquet theory (time domain) The following developments are introduced for the particular 2-dimensional system (87), but they are classical and could be generalized to N -dimensional systems without conceptual difficulties. Since the system (97) is linear with respect to the unknowns $\mathbf{y}(\tau)$, it has $n = 2$ linearly independent solutions $\mathbf{y}_n(\tau)$, so that the general solution $\mathbf{y}(\tau)$ of (97) can be written as

$$\mathbf{y}(\tau) = \sum_{n=1}^2 c_n \mathbf{y}_n(t) \quad (99)$$

where c_n are 2 constants that depend upon the initial conditions and $\mathbf{y}_n(\tau)$ are called fundamental solutions. We gather these into a 2×2 matrix,

$\mathbf{Y}(\tau) = [\mathbf{y}_1(\tau) \ \mathbf{y}_2(\tau)]$. As both $\mathbf{y}_n(\tau)$ verify (97), the fundamental matrix $\mathbf{Y}(\tau)$ also verifies

$$\dot{\mathbf{Y}}(\tau) = \mathbf{J}(\tau)\mathbf{Y}(\tau) \quad (100)$$

and, as $\mathbf{J}(\tau)$ is T -periodic, we have

$$\dot{\mathbf{y}}_n(\tau + T) = \mathbf{J}(\tau + T)\mathbf{y}_n(\tau + T) = \mathbf{J}(\tau)\mathbf{y}_n(\tau + T) \quad (101)$$

so that the $\mathbf{y}_n(\tau + T)$ also verify (97). Consequently the solutions $\mathbf{y}_n(\tau + T)$ can be expressed as linear combinations of the 2 independent fundamental solutions $\mathbf{y}_n(\tau)$. It thus exists a 2×2 constant matrix Φ , called the monodromy matrix, such that:

$$\mathbf{Y}(\tau + T) = \mathbf{Y}(\tau)\Phi. \quad (102)$$

This matrix maps a particular set of fundamental solution $\mathbf{Y}(\tau)$ at time τ into their values at time $\tau + T$ (this map is called a Poincaré map). We therefore use it to study the stability of the straight equilibrium configuration $\mathbf{x}_0 = \mathbf{0}$. We compute its eigenvalues ρ_n and eigenvectors. For an eigenvector of Φ we have, from Eq.(102),

$$\mathbf{y}_n(\tau + T) = \mathbf{y}_n(\tau)\rho_n \quad (103)$$

The ρ_n are therefore called Floquet multipliers which, interestingly, do not depend upon the choice of the fundamental matrix. As a consequence, it is convenient to use the initial conditions $\mathbf{Y}(0) = \mathbf{1}$, where $\mathbf{1}$ is identity matrix. The monodromy matrix then simply reads $\Phi = \mathbf{Y}(T)$, see (102). It is determined by solving the linear system with periodic coefficients (100) over one period $\tau \in (0, T)$ with $\mathbf{Y}(0) = \mathbf{1}$. Moreover, Floquet theory tells us that we can express the fundamental solutions $\mathbf{y}_n(t)$ in the so-called Floquet normal form

$$\mathbf{y}_n(\tau) = \mathbf{r}_n(\tau) e^{s_n \tau} \quad (104)$$

where $\mathbf{r}_n(\tau + T) = \mathbf{r}_n(\tau)$ is a 2-dimensional complex vector of period T and s_n is a complex number called the Floquet exponent (the Floquet form is a generalization of the eigenmodes of vibration defined in (91) for the autonomous system (90)). Then, it follows from Eq.(104) and from the T -periodicity of \mathbf{r}_n that

$$\mathbf{y}_n(\tau + T) = \mathbf{r}_n(\tau + T) e^{s_n(\tau+T)} = \mathbf{y}_n(\tau) e^{s_n T} \quad (105)$$

We therefore see that the Floquet exponents s_n are linked to the Floquet multipliers ρ_n by:

$$\rho_n = e^{s_n T} \Leftrightarrow s_n = \frac{1}{T} \ln \rho_n + \frac{2\pi m}{T} i, \quad m = 0, \pm 1, \pm 2, \dots \quad (106)$$

where $T = \pi$ in our case and i is the unit imaginary number. Whereas the Floquet multipliers are uniquely defined, the above equation shows that the s_n are unique to within an additive integer multiple of $m\omega = 2m\pi/T$ where the fundamental frequency ω reads $\omega = 2\pi/T$. This last result can also be viewed by replacing s_n by $s_n + 2im\pi/T$ in Eq.(106).

Considering Eqs. (103) or (104), the values of either the moduli $|\rho_n|$ of Floquet multipliers or the Floquet exponents s_n are used to determine the stability of the oscillating straight system characterized by \mathbf{x}_0 . The following statements are very similar to Lyapunov's theory previously described except that, in the present case of Floquet theory, the nature of the instability and bifurcations we encounter are different since the perturbed state is periodic and no more constant in time:

- If $\Re(s_n) < 0$ (or $|\rho_n| < 1$) for all n , all fundamental solutions $\mathbf{y}_n(\tau)$ converge toward zero as τ increases, so is any perturbation $\mathbf{y}(\tau)$. The periodic state \mathbf{x}_0 is said to be asymptotically stable;
- If it exists a subscript k such that $\Re(s_k) > 0$ (or $|\rho_k| > 1$), the corresponding fundamental solutions increases exponentially, so are some perturbations $\mathbf{y}(t)$. The periodic state is in this case unstable and three different scenarios have to be considered:
 - If $\Im(s_k) = m\omega$ for $m = 0, \pm 1, \pm 2, \dots$ ($\Im(\rho_k) = 0$ and $\Re(\rho_k) > 0$), the perturbed motion will be a T -periodic oscillation that will exponentially grow in the direction of the k^{th} mode $\mathbf{r}_k(\tau)$ (see Figure 22-Left for the representation in the Argand plane). This loss of stability leads to a steady bifurcation since the perturbed state bifurcates away from the periodic state \mathbf{x}_0 in the state space, but retains its period T .
 - If $\Im(s_k) = \omega/2 + m\omega$ for $m = 0, \pm 1, \pm 2, \dots$ ($\Im(\rho_k) \neq 0$ and $\Re(\rho_k) < 0$), the perturbed motion will be a $2T$ -periodic oscillation that will exponentially grow in the direction of the k^{th} mode $\mathbf{r}_k(\tau)$ (see Figure 22-Center for the representation in the Argand plane). This loss of stability leads to a flip or period-doubling bifurcation: the perturbed state bifurcates both in the state space along $\mathbf{r}_k(\tau)$ and in the time domain (from a T to $2T$ -periodic state). Note that by expressing the periodic state in multiple of $\omega/2$ instead of ω , the flip bifurcation would be transformed in a steady bifurcation. Therefore, flip and steady bifurcation are of same nature.
 - If $\Im(s_k) \neq \omega/2 + m\omega/2$ for $m = 0, \pm 1, \pm 2, \dots$ ($\Im(\rho_k) \neq 0$), the perturbed motion is a periodic or quasi-periodic oscillation that exponentially grows in the direction of the k^{th} mode \mathbf{r}_k (see Figure 22-Right for the representation in the Argand plane). At

least one of the ratio between the frequencies of the perturbation and the fundamental frequency of the perturbed state is not an integer. As a consequence, this instability leads to a secondary Hopf or Nemark-Sacker bifurcation which introduces one or two new frequencies in the bifurcated stationary state. In that case, not only the limit cycle bifurcates in the state space but also in the time domain.

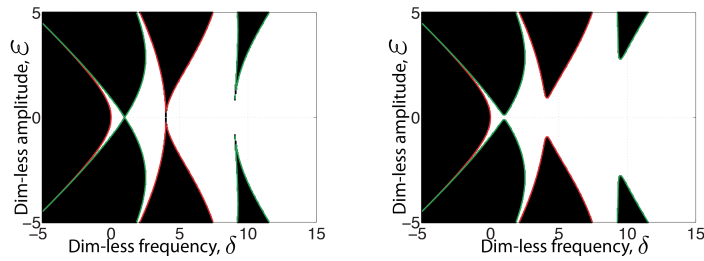


Figure 23. Mathieu’s tongues or stability charts of the vertical solution of the system of Figure 16, in the (δ, ε) plane. Unstable regions are in black. Regions bounded by green and red lines respectively lead to $2T$ and T -periodic steady-state oscillations. (Left) Undamped system with $Q = 10^{10}$, and (Right) Damped system with $Q = 20$.

Numerical applications In this section, we apply Floquet theory to determine the stability of the vertical solution of the system of Figure 16, seen as a periodic state. We compute the Floquet multipliers and exponents of the linearized Eqs.(97)-(98) in the (δ, ε) space. Figure 23-Left and 23-Right show the stability maps of this state in the (δ, ε) plane for $Q = 10^{10}$ (undamped system) and $Q = 20$ respectively. Dark regions are such that the modulus of at least one computed Floquet multiplier is superior to unity. These regions of instability are called Mathieu’s tongues. Their limits have been drawn with colored lines. Green lines surround regions of instability where $2T$ -periodic oscillations develop, while red lines surround regions of instability where T -periodic oscillations develop. Figure 24 gives more details about the shape of Floquet multipliers and exponents for $\varepsilon = 1$ and $Q = 20$ and confirms the alternation between regions of existence of T and $2T$ -periodic solutions. In thin dashed line, we also plot the evolution of the natural frequency of the vertical solution when the base is not moving, i.e the eigenvalues of the constant part of the Jacobian, i.e. \mathbf{J} in Eq. (97) with $\varepsilon = 0$.

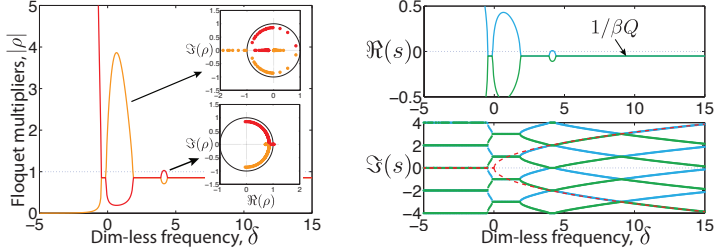


Figure 24. Evolution of Floquet's parameters as a function of dimensionless frequency $\delta = 4\omega_0^2/\Omega^2$ for $Q = 20$ and $\varepsilon = 1$. (Left) Evolution of the modulus of Floquet multipliers. Insets: Evolution of Floquet multipliers in the Argand plane. (Right) Evolution of Floquet exponents. Top: Growth rate. Bottom: Spectrum of the Floquet normal form. Dashed line is the natural frequency of the vertical solution on a standstill base.

Both Figure 23 and Figure 24 give sufficient informations to qualitatively explain the dynamical behavior computed and illustrated in Figure 21. When $\delta < 0$ (i.e. $p > 1$), the vertically oscillating straight configuration is mostly dynamically unstable with the system bifurcating toward a T -periodic solution: in this region, the spectrum of the Floquet exponents shown in Figure 24-Right are locked in the form $\Im(s_k) = m\omega$ for $m = 0, \pm 1, \pm 2, \dots$. Due to the nonlinear term in Eq.(87), the motion consequently settles of a steady-state that is therefore T -periodic. This is what we observe in Figure 21-Left for $\varepsilon = [0.1, 0.4]$ and $p = 1.025$ which corresponds to $\delta = -0.1$. However, there is an interesting narrow region for $\delta < 0$ illustrated in Figure 23, where the vertical solution is a stable periodic state. This counter-intuitive phenomenon can be observed for the couple of parameters $(\delta, \varepsilon) = (-0.1, 0.5)$ for which the dynamical response is given in Figure 21-Left.

When $\delta > 0$, the system in vertical periodic state is a true parametric oscillator. The transverse oscillations of the moving bar are modulated by the harmonic intrinsic motion. As a consequence, there are alternating windows for the parameter $\delta = 4\omega_0^2/\Omega^2$ for which the vertical solution is unstable, even if it is stable in the case of a immobile base ($\varepsilon = 0$). This qualitative behavior is illustrated by the nonlinear dynamic responses in Figure 21-Center and 21-Right where $(\delta, \varepsilon) = (2, 0.1)$ and $(1, 0.1)$ respectively. The first set of parameters leads to a stable straight configuration when the second corresponds to an unstable one. The regions of instability are often called forbidden regions since in those regions, the natural straight

configuration $\theta(\tau) = 0$ is not seen experimentaly. The forbidden regions originate (when $\varepsilon \rightarrow 0$) from particular values $\delta \rightarrow j^2$ with $j = 0, 1, 2, \dots$, i.e. $\Omega = (2/j)\omega_0$. This is specific of parametric instabilities: for particular ratios between the frequency of the forcing and the natural frequency of the unforced system, an eventual amplification of any slight perturbation may happen and give rise to a steady-state oscillation. However, we see from Figure 24-Right that parametric instabilities are not due to resonances, as it is often believed, but rather to an intrinsic frequency lock-in of the spectrum of the Floquet normal forms. From a phenomenological point of view, lock-in is a linear phenomenon where the fundamental frequency $\Im(s_n)$ deviates from the expected natural frequency of the unforced system, given by the dashed line in Figure 24-Right, while being close to secondary harmonics $\Im(s_n) + j\omega$. Since quasi-periodic Floquet forms may have multiple harmonics, multiple lock-in may happen for values of δ close to j^2 with $j = 0, 1, 2, \dots$. Moreover, as the size of the spectrum of the Floquet normal forms decreases with δ (to finally tend to the classic eigenmodes of a structure in equilibrium as $\delta \rightarrow +\infty$), lock-in phenomenon happens mostly for small δ , when Ω and ω_0 are of similar scale, and tends to disappear as δ increases. The first region of instability encountered as δ is increased from zero is called the principal region of instability, when the other ones are referred to as secondary regions of instability. Finally, we note that damping reduces the range of lock-in and therefore the width of forbidden regions for a given set of (δ, ε) .

12 Material instabilities

Energetic methods can be applied in some non-conservative cases. We consider here systems of springs with damage. Damage is an irreversible and dissipative phenomenon. Yet, it is possible to formulate the evolution of damage as an energy minimisation problem under a unilateral constraint representing the irreversibility.

12.1 One spring with damage

We consider a linear spring submitted to a tensile force F . The internal deformation energy of this spring is

$$V_{\text{int}} = \frac{1}{2}k(x - x_0)^2 \quad (107)$$

where k is the stiffness and x the position of the right extremity of the spring. This position is x_0 when no tension ($F = 0$) is applied. In order to model damage happening in the material of the spring, we postulate that

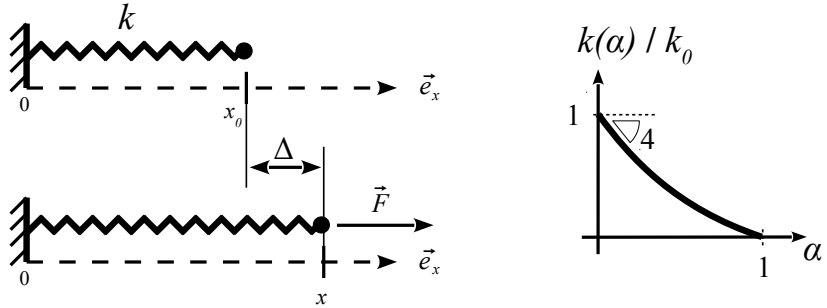


Figure 25. (Left) A damageable spring under tension. During the loading procedure the spring may experience damage and have its stiffness k modified. (Right) The spring stiffness k as function of the damage variable α , see Equation (108).

during a loading experiment the spring stiffness k may decrease

$$k(\alpha) = k_0 \frac{1 - \alpha}{1 + 3\alpha} \quad (108)$$

where the internal variable α accounts for the damage status of the material. The material starts with $\alpha = 0$ and α increases as damage occurs. Damage is considered an irreversible phenomenon and therefore modeled by imposing that the damage variable cannot decrease, $\dot{\alpha} = d\alpha/dt \geq 0$, with time t . When α reaches $\alpha = 1$ the material is ruined. The damage function is such that $k(0) = k_0$ and $k(1) = 0$. Different damage functions $k(\alpha)$ have been considered in the literature, we chose (108) for simplicity reasons. As damage occurs, some energy is dissipated in the system and it is convenient to consider

$$V(x, \alpha) = V_{\text{int}} + V_{\text{dissip}} \quad (109)$$

as the total energy of the system and treat it as conservative. Here we choose $V_{\text{dissip}} = W\alpha$. The dissipation energy W is related to the energy needed to break the spring: as α reaches $\alpha = 1$ the system no longer opposes any reaction to stretching and can be considered broken. We compute the response of the system in a controlled displacement setup, that is we study (109) under the constraint

$$g(x) = (x - x_0) - \Delta \quad (110)$$

where Δ is the imposed displacement. Introducing the augmented energy

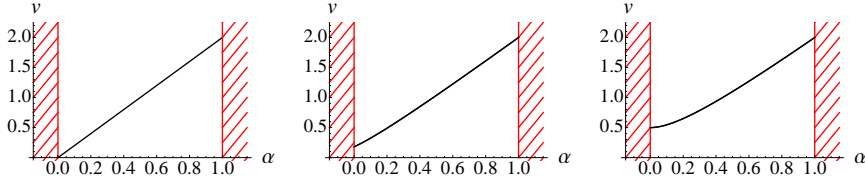


Figure 26. Graphs of the function (113) for (Left) $\epsilon = 0$, (Center) $\epsilon = 0.6$, (Right) $\epsilon = 1$, where $v'(0) = 0$.

$\mathcal{V} = V(x, \alpha) - \lambda g(x)$ and solving for $\partial \mathcal{V}/\partial x = 0$ yields

$$\lambda = k(\alpha) (x - x_0) = F \quad (111)$$

where we identify the Lagrange multiplier λ to the applied tension F . Nevertheless, we use the linearity of the constraint (110) to eliminate the variable x and work with a (unconstrained) one-variable energy

$$V(\alpha) = \frac{1}{2} k_0 \frac{1-\alpha}{1+3\alpha} \Delta^2 + W \alpha \quad (112)$$

We use x_0 as unit length and $k_0 x_0$ as unit force to introduce the dimensionless quantities $\epsilon = \Delta/x_0 = (x - x_0)/x_0$, $w = W/(k_0 x_0^2)$, $f = F/(k_0 x_0)$, and $v = V/(k_0 x_0^2)$. Setting $w = 2$, we obtain

$$v(\alpha) = \frac{1}{2} \frac{1-\alpha}{1+3\alpha} \epsilon^2 + 2\alpha \quad (113)$$

We first consider the loading situation where the extension ϵ is increased quasi-statically from zero, $\epsilon(t) = t$. At each time t we look for the minimum of the energy $v(\alpha)$, under the irreversibility constraint $\dot{\alpha} \geq 0$. We therefore study the graph of $v(\alpha)$ for different values of the imposed parameter ϵ , see Fig. 26. As long as $\epsilon < 1$ the slope at the origin is strictly positive, and the minimum is reached at $\alpha = \alpha^* = 0$. The damage variable does not evolve, the spring experiences no damage. From (111) we compute the force and obtain that, in this first phase, the force f increases linearly with ϵ , $f = \epsilon$.

As $\epsilon > 1$ a second phase starts and the minimum is now reached for $\alpha = \alpha^* > 0$, as seen in the graphs of Figure 27. We solve for $v'(\alpha) = 0$ and find $\alpha^*(t) = (\epsilon - 1)/3 > 1$. The second phase ends at $\epsilon = t = 4$ where the spring is entirely ruined, $\alpha^* = 1$. In this second phase the force f decreases with ϵ :

$$f = 1 - \alpha^* = \frac{4-\epsilon}{3} \quad (114)$$

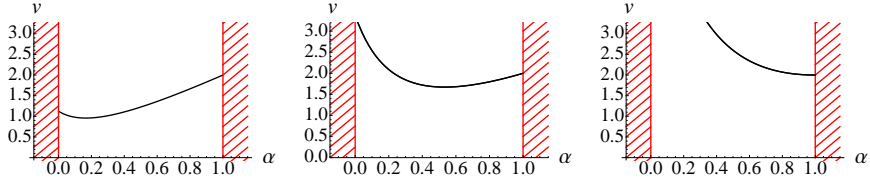


Figure 27. Graphs of the function (113) for (Left) $\epsilon = 1.5$, (Center) $\epsilon = 2.6$, (Right) $\epsilon = 4$, where $v'(1) = 0$.

In summary in the first phase $\dot{\alpha} = 0$ and $v'(\alpha^*) > 0$, while in the second phase $\dot{\alpha} > 0$ and $v'(\alpha^*) = 0$. These two phases correspond to the curves P_1 and P_2 in the force-extension diagram, see Figure 28.

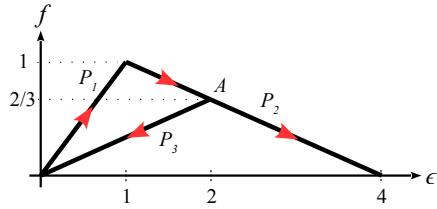


Figure 28. Force-extension diagram for system (113). For paths P_1 and P_2 , the loading is such that $\epsilon(t) = t$. For path P_3 , the loading is such that $\epsilon(t) = 4 - t$, with $t > 2$.

We consider the point A in Figure 28 where $t = 2$ and $\alpha^* = 1/3$, and we reverse the loading: we now impose $\epsilon(t) = 4 - t$. The imposed extension ϵ now decreases from $\epsilon = 2$. Consequently we look for the minimum of $v(\alpha)$ with the condition that α^* cannot decrease under $1/3$. We find that the constraint $\alpha^* \geq 1/3$ is always active: the minimum is reached at $\alpha^* = 1/3$, see Figure 29. The force-extension curve P_3 is plotted in Figure 28.

12.2 Two springs with damage

We now turn to the case where two springs are connected in series, see Figure 30. Following the notations of the previous section, we write the energy of the system as

$$V(\Delta_1, \Delta_2, \alpha_1, \alpha_2) = \frac{1}{2}k(\alpha_1)\Delta_1^2 + \frac{1}{2}k(\alpha_2)\Delta_2^2 + V_{\text{dissip}} \quad (115)$$

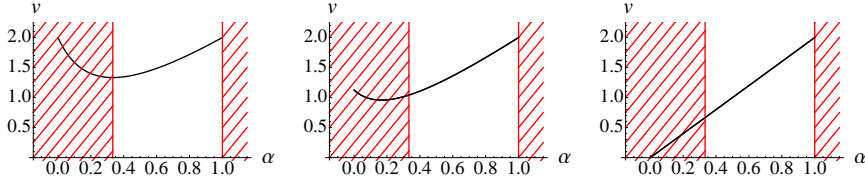


Figure 29. Graph of $v(\alpha)$ during the unloading phase P_3 where $\epsilon = 4 - t$, with $t \in (2, 4)$. According to the past evolution of the system, the minimum of v is searched for $\alpha \geq 1$

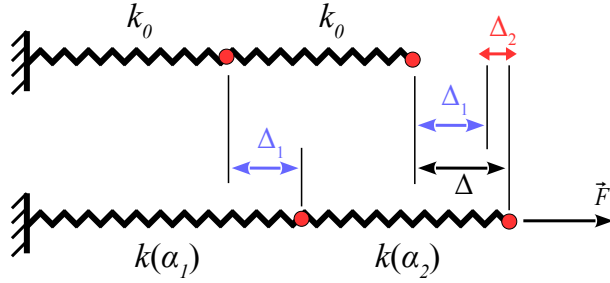


Figure 30. Two damageable springs in series. A displacement Δ is imposed through application of a tension F . During the loading procedure each spring may experience damage and have its stiffness k modified.

where Δ_1 (respectively Δ_2) is the elongation of spring 1 (resp. spring 2). An internal damage variable is associated to each spring and $V_{\text{dissip}} = W\alpha_1 + W\alpha_2$. We study the behavior of the system under controlled displacement, that is under the constraint $\Delta = \Delta_1 + \Delta_2$. As in the one-spring case, pre-minimisation with regard to Δ_1 and Δ_2 yields:

$$F = k(\alpha_1)\Delta_1 = k(\alpha_2)\Delta_2 = k/(\alpha_1, \alpha_2)\Delta \quad (116)$$

with $k/ = [k^{-1}(\alpha_1) + k^{-1}(\alpha_2)]^{-1}$. We use (116) to eliminate Δ_1 and Δ_2 and work with an unconstrained energy $V(\alpha_1, \alpha_2) = \frac{1}{2}k/(\alpha_1, \alpha_2)\Delta^2 + W\alpha_1 + W\alpha_2$ that we non-dimensionalize as in previous section to finally obtain

$$v(\alpha_1, \alpha_2) = \frac{\epsilon^2/2}{\frac{1+3\alpha_1}{1-\alpha_1} + \frac{1+3\alpha_2}{1-\alpha_2}} + 2\alpha_1 + 2\alpha_2 \quad (117)$$

We study $v(\alpha_1, \alpha_2)$ as the parameter $\epsilon(t) = t$ is increased quasi-statically, under the constraints $\dot{\alpha}_1 \geq 0$ and $\dot{\alpha}_2 \geq 0$. We consider discrete time step

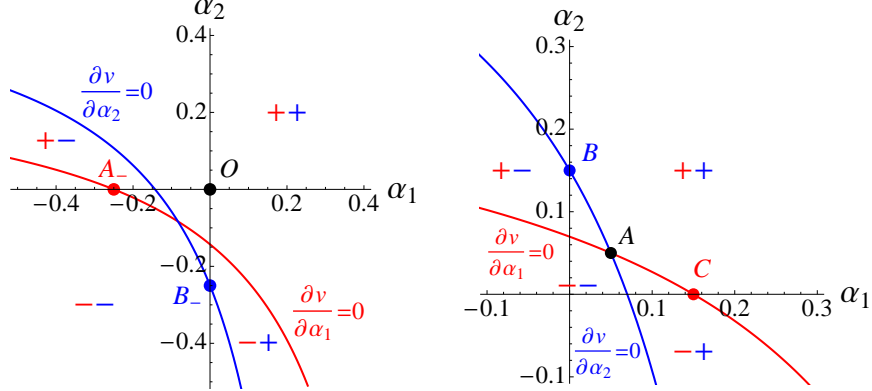


Figure 31. Plane (α_1, α_2) with solutions to (118) with $\epsilon = 1.5$. The curves $\frac{\partial V}{\partial \alpha_i} = 0$ part the plane into regions where the sign of $\frac{\partial V}{\partial \alpha_i}$ is shown, red for $i = 1$, blue for $i = 2$. (Left) Same with $\epsilon = 2.3$

t_i , $i = 0, 1, 2, \dots$. If at time step t_i , the damage variables α_1 and α_2 have reached values α_1^- and α_2^- respectively, we minimize (117) under the inequality constraints $f_1 = \alpha_1 - \alpha_1^- \geq 0$ and $f_2 = \alpha_2 - \alpha_2^- \geq 0$ that is we solve for the Kuhn-Tucker first order necessary conditions (see Section 8)

$$\frac{\partial V}{\partial \alpha_1} = \mu_1, \quad \mu_1 f_1 = 0 \quad (118a)$$

$$\frac{\partial V}{\partial \alpha_2} = \mu_2, \quad \mu_2 f_2 = 0 \quad (118b)$$

where μ_1 (respectively μ_2) is the Lagrange multiplier associated to the constraint $f_1 \geq 0$ (resp. $f_2 \geq 0$). Eq (118) is a system of 4 equations with 4 unknowns $(\alpha_1, \alpha_2, \mu_1, \mu_2)$. Among the solutions we eliminate those having

$$\mu_1 < 0, \mu_2 < 0, f_1 < 0, \text{ or } f_2 < 0 \quad (119)$$

The stability of each of the remaining solution is then assessed separately.

- For $\epsilon < 2$, the solutions to (118) are (i) the origin $(\alpha_1, \alpha_2) = 0$, or (ii) solutions outside the domain $0 \leq \alpha_{1,2} \leq 1$. We represent in Figure 31-Left two such solutions A_- and B_- . Yet we see that point A_- has $\frac{\partial V}{\partial \alpha_1} = \mu_1 = 0$ but $\frac{\partial V}{\partial \alpha_2} = \mu_2 < 0$, and that point B_- has $\frac{\partial V}{\partial \alpha_2} = \mu_2 = 0$ but $\frac{\partial V}{\partial \alpha_1} = \mu_1 < 0$.

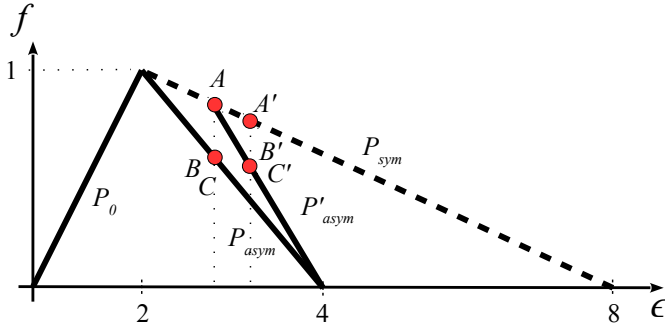


Figure 32. Different paths for the loading of the 2 springs system of Figure (30).

Consequently, in addition to being outside the domain $0 \leq \alpha_{1,2} \leq 1$, points A_- and B_- are eliminated by the test (119). The origin has $\mu_1 > 0$ and $\mu_2 > 0$ and is therefore a local minimum (there is no projected matrix here to test). For this solution the force is $f = 1/2\epsilon$, see path P_0 in Figure 32.

- As ϵ is crossing the threshold $\epsilon = 2$, α_1 and α_2 have not yet evolved from 0 and we have $\alpha_1^- = 0$ and $\alpha_2^- = 0$. The solution to (118) are then (i) $\alpha_1 = \alpha_2 = \frac{\epsilon-2}{6}$ (point A in Figure 31-Right), (ii) $\alpha_1 = 0$ and $\alpha_2 = \frac{\epsilon-2}{2}$ (point B in Figure 31-Right), and (iii) $\alpha_2 = 0$ and $\alpha_1 = \frac{\epsilon-2}{2}$ (point C in Figure 31-Right). Stability of point A , where both constraints f_1 and f_2 are inactive (i.e. $f_1 > 0$ and $f_2 > 0$), is assessed with the Hessian $H_{ij} = \frac{\partial^2 V}{\partial \alpha_i \partial \alpha_j}$ which is found to have one positive $\frac{24}{\epsilon}$ and one negative $\frac{24}{\epsilon-8}$ eigenvalues. Point A is therefore an unstable equilibrium¹. The force is $f = \frac{8-\epsilon}{6}$. Stability of point B , where the constraint f_1 is strongly active ($f_1 = 0$ and $\mu_1(B) = -6 + 4\epsilon - \epsilon^2/2 > 0$ for $2 < \epsilon < 6$) is assessed by testing the projected Hessian or equivalently the second derivative $\frac{\partial^2 v}{\partial \alpha_2^2} = \frac{8}{\epsilon} > 0$. Point B is therefore a stable equilibrium point. The force is $f = \frac{4-\epsilon}{2}$. The same conclusion is reached for point C , which is the symmetrical $\alpha_1 \leftrightarrow \alpha_2$ companion to point B . In conclusion we see that the system either moves toward point B or C and therefore evolves to an unsymmetrical ($\alpha_1 \neq \alpha_2$) state. For subsequent time-steps the system follows the path P_{asym} in

¹We note that we have tested the Hessian for all perturbations on α_1 and α_2 . Different approaches, with a stricter interpretation of the irreversibility conditions, only consider perturbations that let the α values increase. In this latter case point A would be considered stable (Nguyen, 2000).

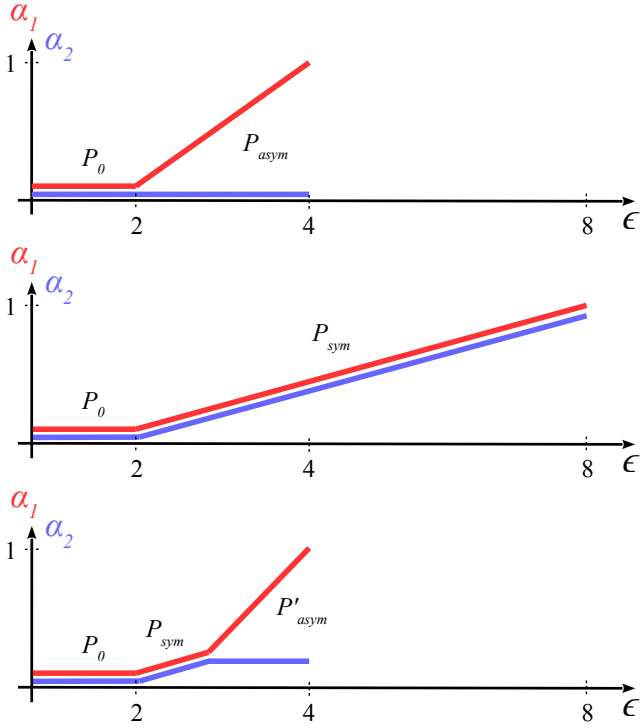


Figure 33. Values of the damage variables along the different paths of Figure (33).

Figure 32. The symmetrical path emerging from point A is labelled P_{sym} in Figure 32.

- For ϵ large than 2, if the system could have evolved along the symmetrical branch P_{sym} , up to say $\alpha_1 = \alpha_2 = \alpha_-$ we would again find 3 solution to (118): (i) a symmetrical unstable solution with $\alpha_1 = \alpha_2 = \frac{\epsilon-2}{6}$ (point A' in Figure 32), (ii) an unsymmetrical stable solution with $\alpha_1 = \alpha_-$ and $\alpha_2 = \frac{2-\epsilon+\alpha_-(\epsilon+2)}{6\alpha_--2}$ where the force is $f = \frac{(\epsilon-4)(1-\alpha_-)}{6\alpha_--2}$ (point B' in Figure 32), and (iii) point C' the symmetrical $\alpha_1 \leftrightarrow \alpha_2$ companion to point B' . These last two point are on path P'_{asym} .

We conclude that in a loading experiment where $\epsilon(t) = t$, the system follows path P_0 up to $\epsilon = 2$ and then path P_{asym} up to $\epsilon = 4$. At $\epsilon = 4$ one of the spring is entirely ruined while the other is undamaged.

Acknowledgments

S.N. thanks Patrick Ballard and Marco Rivetti for discussions, comments, and remarks. Financial support from ANR, through grants ANR-09-JCJC-0022-01, ANR-14-CE07-0023-01, and ANR-13-JS09-0009, as well as from ‘La Ville de Paris - Programme Émergence’ is acknowledged.

Bibliography

- Basile Audoly and Yves Pomeau. *Elasticity and Geometry: From hair curls to the non-linear response of shells*. Oxford University Press, 2010.
- Davide Bigoni. *Nonlinear Solids Mechanics*. Cambridge University Press, 2012.
- V. V. Bolotin. *The dynamic stability of elastic systems*. Holden Day, Inc., 1964.
- G. Domokos and P. Holmes. Euler’s problem, euler’s method, and the standard map; or, the discrete charm of buckling. *Journal of Nonlinear Science*, 3(1):109–151, 1993.
- John Guckenheimer and Philip Holmes. *Nonlinear oscillations, dynamical systems and bifurcations of vector fields*. Springer Verlag, New York, 1983.
- Gérard Iooss and Daniel D. Joseph. *Elementary Stability and Bifurcation Theory*. Undergraduate Texts in Mathematics. Springer Verlag, 1989.
- David G. Luenberger and Yinyu Ye. *Linear and nonlinear programming*. Springer, 3rd edition, 2008.
- Quoc Son Nguyen. *Stability and Nonlinear Solid Mechanics*. John Wiley & Sons, 2000.
- M. Stein. The phenomenon of change in buckle pattern in elastic structures. Technical Report R39, NASA, 1959.
- Steven H. Strogatz. *Nonlinear Dynamics and Chaos, with applications to Physics, Biology, Chemistry and Engineering*. Perseus Publishing, 1994.
- Hans Ziegler. *Principles of Structural Stability*. Springer, Basel AG, 2nd edition, 1977.